PERGAMON

International Journal of Multiphase Flow 27 (2001) 237–276

International Journal of Multiphase Flow

www.elsevier.com/locate/ijmulflow

Flow of spatially non-uniform suspensions Part II: Systematic derivation of closure relations

M. Marchioro, M. Tanksley, W. Wang, A. Prosperetti*, [1]

Department of Mechanical Engineering, The Johns Hopkins University, Baltimore, MD 21218, USA

Received 3 August 1999; received in revised form 6 March 2000

Abstract

This paper presents a systematic method by which closure relations for the ensemble-averaged equations of disperse two-phase flows of solid spheres can be derived. The method relies on the direct numerical simulation of three flow situations: equal forces or couples applied to the spheres, and an imposed macroscopic shear flow. A crucial aspect of the work is that it focuses on systems that are spatially non-uniform on average. It is shown that, due to this feature, several new terms arise in the constitutive relations that would vanish for a uniform system. For example, while the usual effective viscosity is recovered in the closure of the stress tensor, it is found that other terms are also present, which confer a markedly non-Newtonian nature to the rheological constitutive equation.

Keywords: Suspensions; Spatial non-uniformity; Direct numerical simulations; Averaged equations

1. Introduction

In Part I of this work (Marchioro et al., 2000; hereafter referred to as Paper I) we described a method based on direct numerical simulation to characterize the ensemble-average behavior of spatially non-uniform suspensions of spheres at small Reynolds numbers. In the present paper we shall use the results of those simulations to derive *in a systematic manner* constitutive relations for the description of such systems by means of averaged equations. The restriction to

* Corresponding author.

[1] Also Faculty of Applied Physics, Twente Institute of Mechanics, and Burgerscentrum, University of Twente, AE 7500 Enschede, The Netherlands.

0301-9322/01/$ - see front matter
PII: S0301-9322(00)00021-5

small Reynolds numbers is limited to the local scale, rather than to the global macroscopic flow, and therefore, the constitutive relations that we derive are actually applicable also at finite global Reynolds number flows.

We stress the fact that our procedure is systematic and therefore has the capability of producing relations which would be difficult to deduce either experimentally or by a priori considerations. For example, the stress tensor in the mixture is found to be non-Newtonian and non-symmetric. These features are inherently linked to spatial non-uniformities and disappear in the case of a uniform suspension, which explains why they were missed until now. Even though some of the new terms that we find may be small in many cases, they are of great importance in establishing the mathematical structure of the equations (e.g. hyperbolicity, with well-known implications for their numerical solution) and in describing the flow in regions of relatively rapid spatial variations due, for instance, to the accumulation of particles in certain flow structures.

Our method is based on the analysis of direct-simulation results in terms of particular a priori vectors and tensors characterizing each simulation (e.g., an applied force), and on the elimination of these vectors and tensors in terms of averaged quantities (e.g., the mean volumetric flow velocity) so as to obtain *intrinsic* (i.e., at least formally, flow-independent) constitutive relations. Even though systematic, the method is not exact. In the first place, it relies on numerical simulations that we are only able to carry out with limited accuracy. Secondly, we use perturbation tools that give results only accurate to first order in the spatial particle non-uniformity and other non-uniformities induced by it. The first deficiency can readily be remedied with more powerful computational tools. Although the second one can in principle be allayed by carrying more terms in the perturbation expansion, to some extent it is inherent to the method. Nevertheless, the new generation of constitutive relations that we derive, even if possibly of incomplete generality by themselves, should help focus future simulation work and constrain further refinements of constitutive relations.

In spite of the impressive strides made by the direct numerical simulation of disperse multiphase flows (representative recent studies are those by Sangani et al., 1996; Sangani and Mo, 1996; Phung et al., 1996; Stock, 1996; Hu, 1996; Kang et al., 1997; Ladd, 1997; Koch and Ladd, 1997; Morris and Brady, 1998; Ahmed and Elghobashi, 1999; Nobari and Tryggvason, 1996; Pan and Banerjee, 1997; Johnson and Tezduyar, 1997; Glowinsky et al., 1999), it is hard to overestimate the importance of a description in terms of averaged equations. In the first place, the direct numerical simulation of realistic flow situations still belongs to a distant future. Furthermore, even should such calculations be feasible, the staggering amount of detailed information that represents their outcome would often be unnecessary and require massive and complex post-processing — in fact, averaging — to be of practical value. If such averaged quantities could be produced directly, rather than a posteriori, there would be an obvious advantage.

The reason why, after many decades of efforts, the precise form of the averaged equations is still a matter of dispute is that any form of averaging leads to more unknowns than the available equations. Some of the information lost in the averaging process must be reintroduced, and no systematic way of achieving this objective has been devised save in a few highly restricted cases, such as small disperse-phase volume fractions. The fact that our procedure is systematic should therefore be of particular value as it removes — to some extent

at least — the guesswork that has been a prominent feature of this area of investigation for so long.

A detailed description of our techniques is given in Paper I. Here we give a short summary of its salient features not only to enable the present paper to stand by itself but, more importantly, to bring out the essential framework of the study uncluttered by the details that are necessary to explain it fully.

2. The averaged equations

It is necessary to start with a summary of the averaged equations, mixture pressure, mixture stress, and related terms derived in Marchioro et al. (1999); (hereafter referred to as Paper II). In this section we present a very abbreviated treatment, relegating some definitions and other details to Appendix A and directing the reader to the original reference for derivation and analysis.

Both phases are assumed to be individually incompressible and therefore the mean volumetric flow rate $\mathbf{u}_m$, i.e., the ensemble mean velocity at a point, irrespective of the phase occupying that point (see Eq. (A.1)), is divergenceless:

$$\nabla \cdot \mathbf{u}_m = 0. \tag{2.1}$$

The balance equation for the particle number density n is

$$\frac{\partial n}{\partial t} + \nabla \cdot (n\bar{\mathbf{w}}) = 0, \tag{2.2}$$

where $\bar{\mathbf{w}}$ is the ensemble average velocity of the particle center of mass (see Eq. (A.3) for a precise definition). We refer to this type of averages, denoted by an overline, as *particle averages*, to distinguish them from the phase averages introduced later. The particle average is the natural ensemble average for quantities referring to a particle as a whole (such as, here, the center-of-mass velocity), rather than to particle fields (e.g., the average velocity of the particle material at a certain given point $\mathbf{x}$; see Appendix A).

For the purposes of the present work, it is unnecessary to consider the inertia terms of the averaged equations, which are therefore omitted. Upon taking the particle average, the equation of motion for a particle is

$$\overline{\int_{|\mathbf{r}|=a} \mathrm{d}S\boldsymbol{\sigma}_C \cdot \mathbf{n}} + v\rho_D\mathbf{g} = 0. \tag{2.3}$$

Here $v = \frac{4}{3}\pi a^3$, with a the particle radius, is the particle volume and $\boldsymbol{\sigma}_C$ is the microscopic continuous-phase stress tensor, the integral is over the particle surface, and $\mathbf{n}$ is the outwardly directed unit normal; ρ_D is the density of the particle material (assumed uniform) and $\mathbf{g}$ the body force. It was argued in Paper II that it is advantageous to decompose the total hydrodynamic force on the particles — the integral in Eq. (2.3) — into a large-scale (or generalized "pseudo-buoyancy") component and a component $\mathbf{f}$ due to the mean local flow around the particle:

$$\overline{\int_{|r|=a} \mathrm{d}S\boldsymbol{\sigma}_{\mathrm{C}} \cdot \mathbf{n}} = v\nabla \cdot (-p_{\mathrm{m}}\mathbf{I} + \boldsymbol{\Sigma}_{\mathrm{C}}) - v\mathbf{f}. \tag{2.4}$$

The mixture pressure p_{m} and viscous stress $\boldsymbol{\Sigma}_{\mathrm{C}}$ are defined in Eqs. (A.6) and (2.8). It is important to keep in mind that these definitions are phrased solely in terms of the microscopic continuous-phase stress. The analysis of Paper II was based on a study of the transformation properties of the average fields when the microscopic continuous-phase pressure p_{C} is subjected to a gauge transformation, $p_{\mathrm{C}} \rightarrow p_{\mathrm{C}} + \psi$, with ψ an arbitrary harmonic function. It was shown that, while the quantity p_{m} defined in that paper transforms as $p_{\mathrm{m}} \rightarrow p_{\mathrm{m}} + \psi$, both $\boldsymbol{\Sigma}_{\mathrm{C}}$ and $\mathbf{f}$ are invariant under the transformation. As a consequence, one would expect the closure relations for these quantities not to involve in the pressure field.

With the decomposition (2.4) we write the momentum balance for the particles in the unit volume in the form

$$n\nabla(-p_{\mathrm{m}}\mathbf{I} + \boldsymbol{\Sigma}_{\mathrm{C}}) - n\mathbf{f} + n\rho_{\mathrm{D}}\mathbf{g} = 0. \tag{2.5}$$

A general form of the continuous-phase momentum equation is given in Paper II; for the present case in which inertia is negligible and, as shown by Eq. (2.3), the total hydrodynamic force on the particles is a constant, this general form simplifies to

$$\beta_{\mathrm{C}}\nabla(-p_{\mathrm{m}}\mathbf{I} + \boldsymbol{\Sigma}_{\mathrm{C}}) + \beta_{\mathrm{D}}\mathbf{f} + \beta_{\mathrm{C}}\rho_{\mathrm{C}}\mathbf{g} = 0. \tag{2.6}$$

Here $\beta_{\mathrm{C,\,D}}$ are the volume fractions of the continuous and disperse phases defined by

$$\beta_{\mathrm{C,\,D}}(\mathbf{x}, t) = \frac{1}{N!}\int \mathrm{d}\mathscr{C}^{N}\chi_{\mathrm{C,\,D}}(\mathbf{x}; N)P(N; t), \tag{2.7}$$

in which $\chi_{\mathrm{C,\,D}}$ is the characteristic, or indicator, function of the phases. The integral in (2.7) is over the ensemble of configurations of N identical particles distributed according to the probability density $P(N; t)$. Since the particle surface has zero measure, $\chi_{\mathrm{C}} + \chi_{\mathrm{D}} = 1$ and, as a consequence, $\beta_{\mathrm{C}} + \beta_{\mathrm{D}} = 1$. The time variable is unimportant for the present purposes and its explicit indication will be omitted henceforth.

It will be noted that, since β_{D} is not quite equal to nv for a non-uniform suspension, as shown in (A.5), the two momentum equations (2.5) and (2.6) do no precisely satisfy the action–reaction principle. This fact is discussed at length in Paper II, and is a consequence of the use of different averages for the particles in the continuous phase. The reasons for this lack of symmetry in dealing with the two phases are discussed in detail in our earlier work (Zhang and Prosperetti, 1994, 1997; Marchioro et al., 1999, 2000). It is explicitly shown in Paper II that, when the particle average is reduced to the phase average for the disperse phase, the action–reaction principle is precisely satisfied.

It is shown in Paper II and in Appendix A that the average viscous stress in the mixture, $\boldsymbol{\Sigma}_{\mathrm{C}}$, can be decomposed as

$$(\boldsymbol{\Sigma}_{\mathrm{C}})_{ij} = -q_{\mathrm{m}}\delta_{ij} + \mathsf{S}_{ij} + \varepsilon_{ijl}\left(\mathsf{R}_{l} - \varepsilon_{lqr}\partial_{q}\mathsf{V}_{r}\right), \tag{2.8}$$

where q_{m} is a scalar, S a symmetric tensor, R a pseudo-vector, and V a vector. All these quantities can be expressed explicitly in terms of particle averages of quantities that are

computed from the results of the numerical simulations. Explicit expressions are given in Appendix B.

In the following it will be seen that an equation for the angular velocity of the particle phase is also necessary. Neglecting inertia, this equation is (Zhang and Prosperetti, 1997)

$$a\overline{\int_{|\mathbf{r}|=a} \mathrm{d}\mathsf{S}\, \mathbf{n}\times(\boldsymbol{\sigma}_{\mathrm{C}}\cdot\mathbf{n})} + \bar{\mathbf{T}} = 0, \tag{2.9}$$

where $\bar{\mathbf{T}}$ is the mean external couple acting on the particles.

The quantities to be closed are q_{m}, S, R, V, $\mathbf{f}$, and the mean hydrodynamic couple (first term in Eq. (2.9)). It should be explicitly noted that all these quantities are invariant under a gauge transformation of the pressure.

3. Method of closure

The momentum balances as written in the previous section involve more quantities than there are equations for. This is the well-known closure problem that plagues any attempt at deriving averaged equations. Here we describe the principle of the method by which we shall systematically derive — rather than "guess" — closure relations relating the auxiliary variables expressed in terms of averages to the fundamental average fields that we take to be β_{D}, p_{m}, $\mathbf{u}_{\mathrm{m}}$, and $\bar{\mathbf{w}}$ and the mean particle angular velocity $\bar{\boldsymbol{\Omega}}$.

Our method is based on a numerical implementation of the ensemble averaging principle: many realization of the same macroscopic flow are generated numerically and the results are then averaged.

In broad outline, the approach is as follows. Let a particular flow be characterized by parameters $q_1, q_2, \ldots, q_{K-1}$. In practice, these quantities could specify a characteristic spatial scale, an applied force, and so forth. All the average quantities that arise in the numerical solution of the problem, such as, the mean volumetric flow velocity $\mathbf{u}_{\mathrm{m}}$, the mean center-of-mass velocity of the particles $\bar{\mathbf{w}}$, the mixture stress $\boldsymbol{\Sigma}_{\mathrm{C}}$, etc. will then also be functions of the same parameters:

$$\mathbf{u}_{\mathrm{m}} = \mathbf{u}_{\mathrm{m}}(\mathbf{x}; q_1, q_2, \ldots, q_{K-1}), \tag{3.1a}$$

$$\bar{\mathbf{w}} = \bar{\mathbf{w}}(\mathbf{x}; q_1, q_2, \ldots, q_{K-1}), \tag{3.1b}$$

$$\boldsymbol{\Sigma}_{\mathrm{C}} = \boldsymbol{\Sigma}_{\mathrm{C}}(\mathbf{x}; q_1, q_2, \ldots, q_{K-1}), \tag{3.1c}$$

Choose K quantities as primary (e.g. pressure, velocities, volume fraction, etc.). By eliminating $\mathbf{x}$ and the q_j's between these K primary quantities and the remaining ones, a series of functional relations is obtained that are, at least formally, problem independent:

$$\boldsymbol{\Sigma}_{\mathrm{C}} = \boldsymbol{\Sigma}_{\mathrm{C}}(\mathbf{u}_{\mathrm{m}}, \bar{\mathbf{w}}, \ldots). \tag{3.2}$$

If these relations are indeed intrinsic constitutive, the particular problem or parameters that

have been used to derive them are of no particular importance and can, therefore, be chosen with convenience in mind.

It is of course by no means obvious that such intrinsic constitutive relations exist, but certainly, if they do not, any averaged description of the system is impossible. Hence, we proceed on the heuristic assumption that, at least in some approximate sense that has a practically useful domain of applicability, they do exist.

The steps in implementing the above procedure consist therefore in deriving the parameterizations (3.1) for one or more selected flows, compute the coefficients that appear in these relations by numerical simulation, and carry our the elimination process leading to Eq. (3.2) for all the necessary average quantities.

It will be seen that, in order to carry out this program, it is necessary to simulate spatially non-uniform suspensions. The method by which this is achieved has been explained in Paper I and need not be repeated here.

4. Numerical simulations

In order to simulate an infinite suspension, we use the well-known device of filling up space with copies of a fundamental cubic cell of side L (see e.g. Sangani and Yao, 1988; Mo and Sangani, 1994). For each volume fraction, we generate a large number of configurations by randomly arranging N particles in the cell. As described in Paper I, we have satisfied ourselves that the two-particle distribution function calculated on the configurations of these ensembles is in very good agreement with the known result for hard spheres (see e.g. Throop and Bearman, 1965). We have also calculated the nearest-neighbor distribution function and the static structure factor, finding results in agreement with those in the literature (see e.g. Torquato and Lee, 1990; Studart et al., 1996).

The exact microscopic velocity and pressure fields in the suspension are written in the form

$$\mathbf{u}_{\mathrm{C}} = \mathbf{U}_{\infty} + \tilde{\mathbf{u}}_{\mathrm{C}}, \qquad p_{\mathrm{C}} = P_{\infty} + \tilde{p}_{\mathrm{C}} \tag{4.1}$$

where $\mathbf{U}_{\infty}$ and P_{∞} are imposed velocity and pressure fields and $\tilde{u}_{\mathrm{C}}$, $\tilde{p}_{\mathrm{C}}$ have the same periodicity as the fundamental cell (Mo and Sangani, 1994). These fields are calculated by the method of Mo and Sangani (1994), briefly summarized in Paper I (see also Appendix B). In all the situations that we consider, $\nabla^2 \mathbf{U}_{\infty} = 0$.

As described in detail in Paper I, on the ensembles that we have generated we construct a slightly non-uniform probability distribution characterized by a sinusoidal variation

$$\sin \mathbf{k} \cdot \mathbf{x}, \tag{4.2}$$

where $|\mathbf{k}| = 2\pi/L$ and the direction of $\mathbf{k}$ is taken along one of the sides of the cell. The resulting number density is

$$n = n^0 + \epsilon n^s \sin \mathbf{k} \cdot \mathbf{x}, \tag{4.3}$$

where n^0 and n^s are constants dependent on the volume fraction and cell size and $|\epsilon| \ll 1$. Similarly,

$$\beta_{\mathrm{D}} = \beta_{\mathrm{D}}^{0} + \epsilon\beta_{\mathrm{D}}^{s}\sin \mathbf{k}\cdot\mathbf{x}. \tag{4.4}$$

The sinusoidal spatial dependence exhibited by these relations applies to all the average fields, generally including also a term proportional to $\epsilon\cos \mathbf{k}\cdot\mathbf{x}$ that happens to vanish in the expressions for n and β_{D}. Note that since, on the particle scale, L is large, the spatial variation expressed by relations such as (4.3) is slow when measured on the scale a. Note also that, since the average fields (with the exception of the pressure) depend sinusoidally on position (see e.g. (4.3)), every derivative introduces an additional power of $k = 2\pi/L$.

The spatially periodic structure that we rely upon plays a two-fold role, one useful — the introduction of a controlled spatial non-uniformity — and one undesirable, namely the possible contamination of this spatial non-uniformity by spurious consequences of the underlying repetition of the unit cell. In some cases, these two sources of k-dependence can be separated. For example, the factor k^2 that would arise upon calculating $\nabla^2\beta_{\mathrm{D}}$ from Eq. (4.4) is evidently solely due to the spatial non-uniformity. Conversely, a k-dependence encountered in quantities calculated for a spatially uniform system must be an artifact of the periodic structure. An example given in Paper I is the hindered settling function for sedimentation (Fig. 4 of Paper I); Mo and Sangani (1994) find a similar dependence for the permeability of a porous medium. On the other hand, this artifact is sometimes absent as found in the case of the effective viscosity for simple shear (solid lines in Fig. 17 of Paper I), which turns out to be independent of cell size. When the k-dependence appears upon plotting the numerically

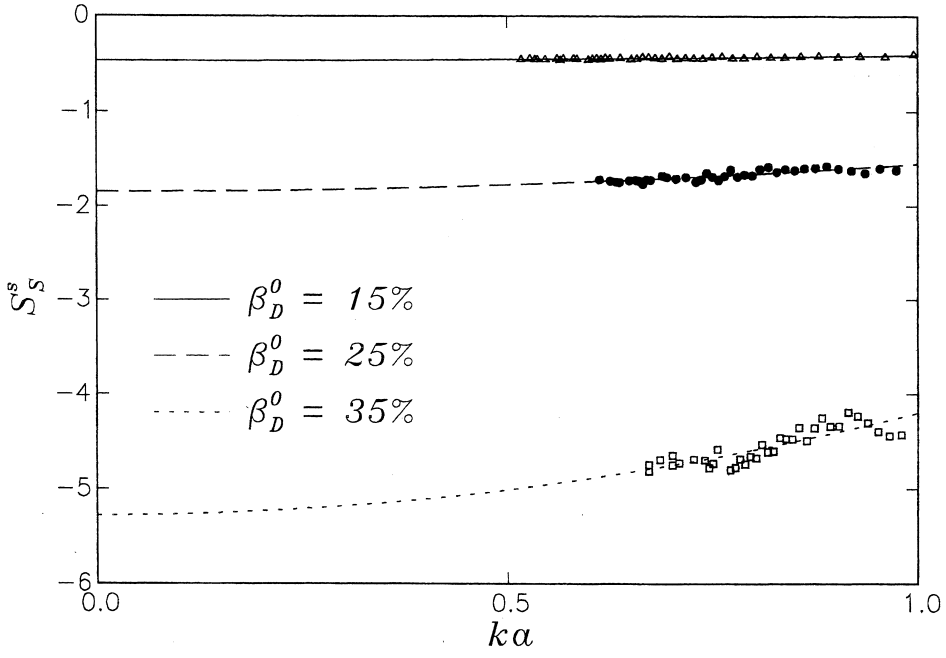

Fig. 1. The quantity s_S^s defined in Eq. (6.10) as a function of ka for $\beta_{\mathrm{D}}^0 = 15\%$ (triangles), 25% (black circles), and 35% (squares); the lines are least-squares fits of the form $A + B(ak)^2$.

computed coefficients as functions of ka in terms related to the spatial non-uniformity (see e.g. Figs. 1 and 2 and the text following Eq. (6.10)), however, an ambiguity exists.

In principle, to avoid this contamination of the k-dependence of the quantities we calculate, one could repeat the averaging with non-uniformities having wavenumber $2\mathbf{k}$, $3\mathbf{k}$, etc., and try to separate in this way the k-dependence genuinely due to the spatial non-uniformity. Unfortunately, convergence of the averages when the wavelength is decreased becomes very slow, and this approach is impractical with our current computational resources. Thus, in this paper, we shall mainly rely on results obtained in the limit $k \to 0$ for a fixed volume fraction. Since, as is easily shown,

$$ka = \left(\frac{6\pi^2}{N}\beta_{\mathrm{D}}^0\right)^{1/3}, \tag{4.5}$$

for each value of β_{D}^0, this extrapolation requires simulations with different numbers N of particle in the cell, from a minimum of about 10 to a maximum of about 60. The range of values of ka that we are able to cover is therefore from about 0.5 to 1.

Three distinct physical situations have been simulated. In the first one, the motion of the particles is induced by a body force $\mathbf{g}$ and $\mathbf{U}_\infty$ is an arbitrary rigid-body motion. Under the action of this force, an isolated spherical particle of radius a would move with the velocity

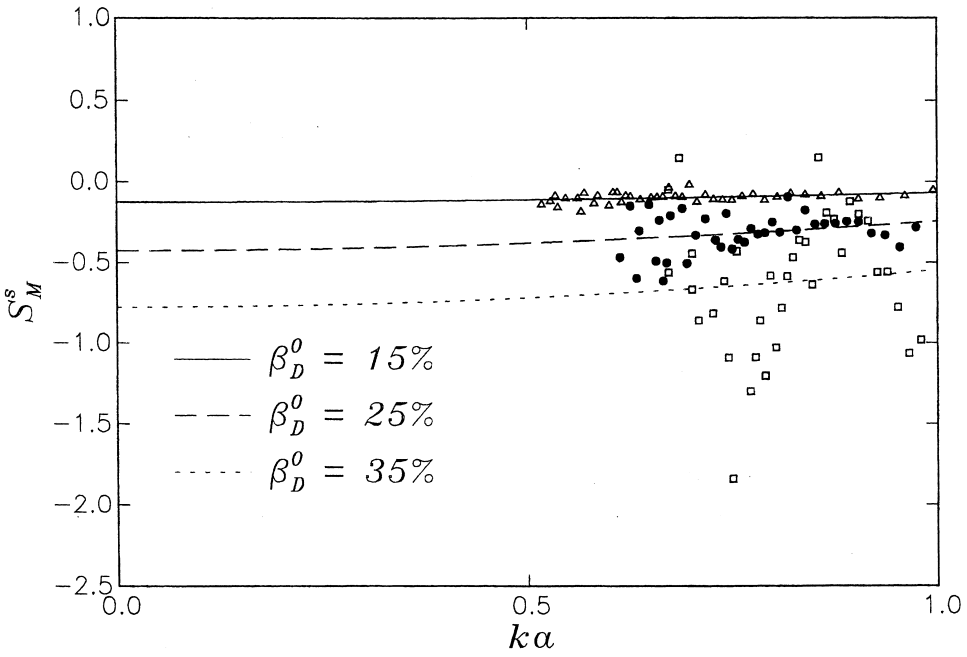

Fig. 2. The quantity s_M^s defined in Eq. (6.10) as a function of ka for $\beta_{\mathrm{D}}^0 = 15\%$ (triangles), 25% (black circles), and 35% (squares); the lines are least-squares fits of the form $A + B(ak)^2$.

$$\mathbf{W} - \mathbf{U}_\infty = \frac{2}{9}\frac{\rho_D - \rho_C}{\mu_C} a^2 \mathbf{g}. \tag{4.6}$$

The second flow is induced by an imposed simple shear characterized, up to an arbitrary rigid-body motion, by

$$\mathbf{U}_\infty = \boldsymbol{\gamma} \cdot \mathbf{x}, \tag{4.7}$$

with $\boldsymbol{\gamma}$ being a symmetric traceless constant two-tensor. The third situation considered is one in which each particle is subject to a couple $\mathbf{T}$ under the action of which an isolated particle would rotate with the angular velocity

$$\boldsymbol{\omega} - \frac{1}{2}\nabla \times \mathbf{U}_\infty = \frac{1}{6v\mu_C}\mathbf{T}, \tag{4.8}$$

where, again, $\mathbf{U}_\infty$ is an arbitrary rigid-body motion. In the last two simulations, we take $\mathbf{g} = 0$.

For each configuration of the ensemble, we impose on the system in turn the three perturbing agents mentioned before and calculate the multipole coefficients describing the flow around each sphere (see Appendix B and Mo and Sangani, 1994). Since we are dealing with Stokes flow, it is not necessary to follow the evolution of the system in time, as the entire flow only depends on the instantaneous configuration of the spheres.

Some details on the method of numerical simulation used to generate the present results are given in Paper I and will not be repeated here. It will suffice to say that we use the method described in Mo and Sangani (1994), whose code has been substantially rewritten and developed. Naturally, we have made sure that the results given by the original code and our code coincided. The particles were represented by five singularities. In some cases, six singularities were used finding essentially identical results at the two lower volume fractions of 15 and 25%, but some differences at the highest volume fraction of 35%. Unfortunately, the computational resources at our disposal prevented us from using six singularities for all cases.

One of the obstacles encountered in this work has been the slowness of convergence of the average quantities related to the spatial non-uniformity. All the results that are shown below are based on the average of results for at least 1000 configuration for each value of β_D^0 and each value of ak. Thus, the total number of individual simulations that we have conducted for this work is well in excess of 100,000. In spite of this effort, in some cases the residual numerical scatter suggests that it would be desirable to average over an even larger number of configurations. Before doing so, it seems reasonable to wait for better numerical methods and computing hardware, particularly in view of the need to extrapolate to $ka = 0$. The chief aim of this work is to describe the method; the actual numerical results presented should be regarded as preliminary. We hope to be able to refine the present calculations in the near future by means of a new simulation method currently under development in our group.

5. Primary and derived variables

According to the plan outlined in Section 3, we need to identify a set of primary averaged quantities in terms of which to express all the closure quantities. The motion of a volume

element of the suspension is defined by the mean volumetric flux $\mathbf{u}_m - \mathbf{U}_\infty$. The mean particle motion relative to $\mathbf{u}_m$ will be described in terms of the interphase "slip" velocity

$$\mathbf{u}_\Delta = \bar{\mathbf{w}} - \mathbf{u}_m, \tag{5.1}$$

and the mean particle rotation relative to the mixture by the interphase slip angular velocity

$$\boldsymbol{\Omega}_\Delta = \bar{\boldsymbol{\Omega}} - \frac{1}{2}\nabla \times \mathbf{u}_m, \tag{5.2}$$

both these vectors being objective. The local composition of the suspension is specified by the disperse-phase volume fraction β_D. The two continuity equations (2.1) and (2.2), the momentum equations (2.5) and (2.6), and the angular momentum balance (2.9) constitute a set of five equations from which $\mathbf{u}_m$, $\mathbf{u}_\Delta$, β_D, $\boldsymbol{\Omega}_\Delta$, and the mean pressure p_m can be determined. It may be noted that this formulation is similar to that of the widely used two-fluid models. In terms of these primary variables, we can construct a certain number of scalars, vectors, and tensors that will be used in the closure, as follows.

5.1. Polar and axial vectors

The only Galilean invariant polar vector with no derivatives available for the closure is the slip velocity $\mathbf{u}_\Delta$. Vectors like $\mathbf{u}_m - \mathbf{U}_\infty$ or $\bar{\mathbf{w}} - \mathbf{U}_\infty$ would be Galilean-invariant, but $\mathbf{U}_\infty$ is a simulation-dependent quantity, and therefore, cannot be allowed in the closure relations as discussed in Section 3.

With one derivative one can form the polar vectors $\nabla\beta_D$ and ∇p_m; since the latter is not invariant under a gauge transformation of the pressure, however, it cannot be used for the closure of gauge-invariant quantities (see Paper II). Two other admissible polar vectors with one derivative are

$$\nabla \times \boldsymbol{\Omega}_\Delta, \qquad \boldsymbol{\Omega}_\Delta \times \nabla\beta_D. \tag{5.3}$$

Two possible vectors with two derivatives are

$$\nabla^2\mathbf{u}_m, \qquad \nabla\beta_D \cdot \mathbf{E}_m, \tag{5.4}$$

where $\mathbf{E}_m$ is the rate of strain of the mean volumetric flow rate $\mathbf{u}_m$:

$$\mathbf{E}_m = \frac{1}{2}\left[\nabla\mathbf{u}_m + (\nabla\mathbf{u}_m)^T\right], \tag{5.5}$$

with the superscript T denoting the transpose. With two derivatives, from $\mathbf{u}_\Delta$ and β_D we can also construct

$$\nabla(\nabla \cdot \mathbf{u}_\Delta), \quad \nabla^2\mathbf{u}_\Delta, \quad \mathbf{u}_\Delta\nabla^2\beta_D, \quad (\mathbf{u}_\Delta \cdot \nabla)\nabla\beta_D. \tag{5.6}$$

Terms analogous to the last two with $\mathbf{u}_m$ in place of $\mathbf{u}_\Delta$ cannot be used for closure as they are not Galilean invariant; a term analogous to the first one would vanish by Eq. (2.1). A term of the form $(\nabla\beta_D \cdot \nabla)\mathbf{u}_\Delta$ is of the order ϵ^2 and cannot be determined by our method.

As already mentioned, all the average fields depend sinusoidally on position (see e.g. (4.3))) and therefore every derivative introduces an additional power of $k = 2\pi/L$. Since, on the particle scale, L is large, we may think that any additional derivative reduces the order of magnitude of a quantity by one order in k. It may be recalled from Paper I that, as $k \to 0$, $\mathbf{u}_m$ diverges as $1/k^2$ for the case of sedimentation and as $1/k$ for the applied shear. For this reason, both vectors (5.4) are of order 1 or k as $k \to 0$. On the other hand, $\mathbf{u}_\Delta$ is finite for $k \to 0$ and therefore all the terms in (5.6) are of order k^2 in the present simulations.

By similar arguments, admissible axial vectors are

$$\begin{aligned} &\boldsymbol{\Omega}_\Delta, \quad \boldsymbol{\Omega}_\Delta \nabla^2 \beta_D, \quad \nabla^2 \boldsymbol{\Omega}_\Delta, \quad \nabla(\nabla \cdot \boldsymbol{\Omega}_\Delta), \quad (\boldsymbol{\Omega}_\Delta \cdot \nabla)\nabla\beta_D, \quad \nabla \times \left(\mathbf{E}_m \cdot \nabla \beta_D\right), \quad \nabla^2(\nabla \times \mathbf{u}_m) \\ &\nabla \times \mathbf{u}_\Delta, \quad \mathbf{u}_\Delta \times \nabla \beta_D, \end{aligned} \tag{5.7}$$

but not the corresponding expressions with $\mathbf{u}_m$ in place of $\mathbf{u}_\Delta$ due to lack of objectivity and Galilean invariance. We do not include a term such as $\nabla^2(\nabla \times \mathbf{u}_\Delta)$, which is at least of order k^3.

5.2. Symmetric tensors

In addition to $\mathbf{E}_m$, the available traceless symmetric tensors are the rate of strain of the slip velocity

$$\mathbf{E}_\Delta = \frac{1}{2}\left[\nabla \mathbf{u}_\Delta + (\nabla \mathbf{u}_\Delta)^T\right] - \frac{1}{3}(\nabla \cdot \mathbf{u}_\Delta)\mathbf{I}, \tag{5.8}$$

and

$$\mathbf{E}_\nabla = \frac{1}{2}\left[\mathbf{u}_\Delta \nabla \beta_D + \left(\mathbf{u}_\Delta \nabla \beta_D\right)^T\right] - \frac{1}{3}\left(\mathbf{u}_\Delta \cdot \nabla \beta_D\right)\mathbf{I}, \tag{5.9}$$

$$\nabla^2 \mathbf{E}_m, \qquad \mathbf{E}_m \nabla^2 \beta_D. \tag{5.10}$$

Since antisymmetric two-tensors are expressible in terms of axial vectors, we shall have no need for them. For the reasons noted before, we do not include tensors constructed with higher-order derivatives.

5.3. Scalars

Aside from β_D and p_m, the only scalars available for the closure relations are

$$\nabla \cdot \mathbf{u}_\Delta, \qquad \mathbf{u}_\Delta \cdot \nabla \beta_D. \tag{5.11}$$

As pointed out in Section 7, it is not necessary to include terms with higher-order derivatives.

6. Symmetric part of the viscous stress

As expression for the viscous stress S is given in Eq. (A.8) of Appendix A. This definition is in terms of averages of the local fields which are computed from the results of the numerical simulations. Thus, S can be considered as known in a form analogous to Eq. (3.1c). The task that we now undertake is to derive a closure relation for it by expressing it in a form analogous to Eq. (3.2).

The tensor S is symmetric and traceless and must therefore be expressed in terms of tensors of a similar nature. On the basis of the linearity constraint applicable to the present case of Stokes flow and of the considerations of the previous section, we therefore write

$$\mathsf{S} = 2\mu_{\mathrm{eff}}\mathbf{E}_{\mathrm{m}} + 2\mu_{\Delta}\mathbf{E}_{\Delta} + 2\mu_{\nabla}\mathbf{E}_{\nabla} + 2\mu_1 a^2\mathbf{E}_{\mathrm{m}}\nabla^2\beta_{\mathrm{D}} + 2\mu_0 a^2\nabla^2\mathbf{E}_{\mathrm{m}}, \tag{6.1}$$

and try to determine the coefficients in a consistent way from the numerical results of the simulations.

Upon taking the divergence of S as given by Eq. (6.1), one would end up with fifth-order derivatives of the velocities in the averaged momentum equation. Without getting into the complex (and not fully resolved) question of the appropriate boundary conditions for the two-fluid model, it is clear that, unless a new class of boundary conditions were formulated, it would not be possible to solve such high-order equations. If one were to limit the theory to the customary second-order velocity derivatives in the momentum equation, the last two terms in Eq. (6.1) should be considered of higher order and dropped. The reason why we do not do so quite yet will be clear from the considerations that follow.

An unfortunate but unavoidable feature of the analysis that follows is the appearance of a large number of coefficients that must be evaluated numerically. In order to avoid lengthy repetitions, we rely on the results of Paper I to which the reader can refer for definitions. For clarity, it is best to first consider separately the cases of an imposed shear, sedimentation, and applied couple deriving the appropriate relations from which the effective viscosities are to be found. After this step, we shall consider the problem of solving these equations.

6.1. Shear

Using the results of Section 9 of Paper I we write

$$\mathbf{u}_{\mathrm{m}} = \boldsymbol{\gamma}\cdot\mathbf{x} + \frac{U^c}{k}\epsilon_c\boldsymbol{\gamma}^{\perp}, \tag{6.2}$$

$$\mathbf{u}_{\Delta} = a^2 k\left(u_{\perp}^c\boldsymbol{\gamma}^{\perp} + u_{\parallel}^c\boldsymbol{\gamma}^{\parallel}\right)\epsilon_c, \tag{6.3}$$

where

$$\boldsymbol{\gamma}^{\parallel} = (\mathbf{m}\cdot\boldsymbol{\gamma}\cdot\mathbf{m})\mathbf{m}, \qquad \boldsymbol{\gamma}^{\perp} = \boldsymbol{\gamma}\cdot\mathbf{m} - (\mathbf{m}\cdot\boldsymbol{\gamma}\cdot\mathbf{m})\mathbf{m}, \tag{6.4}$$

$$\mathbf{m} = \frac{\mathbf{k}}{k}, \tag{6.5}$$

$$\epsilon_s = \epsilon \sin \mathbf{k} \cdot \mathbf{x}, \qquad \epsilon_c = \epsilon \cos \mathbf{k} \cdot \mathbf{x}. \tag{6.6}$$

As shown in Paper I, the coefficients U^c, $u^c_\perp$, $u^c_\parallel$ appearing here are finite in the limit $k \to 0$.

From Eqs. (6.2) and (6.3) we can calculate the tensors that arise in the right-hand side of Eq. (6.1). Before substituting these results into Eq. (6.1), it is important to note that $\mathbf{E}_\mathrm{m}$ is $O(1)$ rather than $O(\epsilon)$. Since all the viscosities, and in particular μ_eff, are a function of $\beta_\mathrm{D} = \beta^0_\mathrm{D} + \beta^s_\mathrm{D}\epsilon_s$, we have

$$\mu_\mathrm{eff}(\beta_\mathrm{D})\mathbf{E}_\mathrm{m} = \left[\mu_\mathrm{eff}\left(\beta^0_\mathrm{D}\right) + \frac{\mathrm{d}\mu_\mathrm{eff}}{\mathrm{d}\beta_\mathrm{D}}\beta^s_\mathrm{D}\epsilon_s\right]\mathbf{E}_\mathrm{m} + O(\epsilon^2). \tag{6.7}$$

We can now proceed with the substitution of the expressions for $\mathbf{E}_\mathrm{m}$, $\mathbf{E}_\Delta$ etc. into Eq. (6.1) to find

$$\begin{aligned} \mathsf{S} = {} & 2\left[\mu_\mathrm{eff} + \beta^s_\mathrm{D}\left(\frac{\mathrm{d}\mu_\mathrm{eff}}{\mathrm{d}\beta_\mathrm{D}} - a^2k^2\mu_1\right)\epsilon_s\right]\boldsymbol{\gamma} - 2a^2k^2u^c_\parallel\mu_\Delta\epsilon_s\mathbf{G}^\gamma_M \\ & - 2\left[\mu_\mathrm{eff}U^c + a^2k^2\left(\mu_\Delta u^c_\perp - \mu_0 U^c\right)\right]\epsilon_s\mathbf{G}^\gamma_S, \end{aligned} \tag{6.8}$$

where

$$\mathbf{G}^\gamma_M = \left(\boldsymbol{\gamma}^\parallel \cdot \mathbf{m}\right)\left(\mathbf{mm} - \frac{1}{3}\mathbf{I}\right), \qquad \mathbf{G}^\gamma_S = \gamma^\perp\mathbf{m} + \mathbf{m}\boldsymbol{\gamma}^\perp. \tag{6.9}$$

On the other hand, S can be calculated directly from its definition (A.8) in terms of ensemble averages of the multiple coefficients of the local expansion of the fields near the particles. On the basis of considerations similar to those described in Marchioro and Prosperetti (1999), it is found that the numerical results thus obtained can be parameterized in the same way as in the right-hand side of Eq. (6.8):

$$\frac{1}{\mu_\mathrm{C}}\mathsf{S} = \left(s^0 + s^s\epsilon_s\right)\boldsymbol{\gamma} + s^s_S\epsilon_s\mathbf{G}^\gamma_S + a^2k^2s^s_M\epsilon_s\mathbf{G}^\gamma_M. \tag{6.10}$$

We stress again that the coefficients s are to be considered known as a result of the numerical simulations. In order to give an idea of the character of these numerical results, Figs. 1 and 2 show graphs of s^s_S and s^s_M as functions of ka for $\beta^0_\mathrm{D} = 15\%$ (triangles), 25% (black circles), and 35% (squares); the lines are least-squares fits of the form $A + B(ak)^2$. It is seen that the results for s^s_S are smooth and reasonably well fitted; for s^c_M the 15% results are smooth, while the higher-β^0_D ones exhibit irregularities probably due to an incomplete convergence of the mean. These two figures are typical of the numerical results that we encounter; further examples can be found in Paper I.

If Eqs. (6.8) and (6.10) hold simultaneously, it is necessary that

$$\frac{\mu_{\text{eff}}}{\mu_{\text{C}}} = \frac{1}{2}s^0, \tag{6.11}$$

$$\frac{\mathrm{d}}{\mathrm{d}\beta_{\text{D}}}\left(\frac{\mu_{\text{eff}}}{\mu_{\text{C}}}\right) - a^2k^2\frac{\mu_1}{\mu_{\text{C}}} = \frac{1}{2}\frac{s^s}{\beta_{\text{D}}^s}, \tag{6.12}$$

$$\frac{\mu_{\text{eff}}}{\mu_{\text{C}}}U^c + a^2k^2\left(\frac{\mu_\Delta}{\mu_{\text{C}}}u_\perp^c - \frac{\mu_0}{\mu_{\text{C}}}U^c\right) = -s_S^s \tag{6.13}$$

$$-2\frac{\mu_\Delta}{\mu_{\text{C}}}u_\parallel^c = s_M^s. \tag{6.14}$$

A consideration of these equations justifies the retention of higher-order derivatives in our closure equation (6.1) since we see here that μ_Δ appears to be in the same order in k as μ_0. Thus, even if the term μ_0 is eventually to be disregarded in the averaged equations, if it had been dropped in writing Eq. (6.1), the numerical value of μ_Δ would be calculated incorrectly; a similar situation is encountered for the case of sedimentation. This peculiarity arises because of the rather artificial nature of the situations that we simulate, which leads to some coefficients diverging in the limit $k\to 0$ (see e.g. (6.2) and the considerations in Paper I). This feature would not be present in the simulation of more physical flows, to which therefore terms such as $\mathbf{E}_{\text{m}}\nabla^2\beta_{\text{D}}$ and $\nabla^2 E_{\text{m}}$ would not be expected to contribute significantly.

6.2. Sedimentation

From Section 8 of Paper I we write

$$\mathbf{u}_{\text{m}} - \mathbf{U}_\infty = \frac{U^s}{a^2k^2}\epsilon_s\mathbf{W}^\perp, \tag{6.15}$$

$$\mathbf{u}_\Delta = \Phi^0\mathbf{W} + u_\perp^s\epsilon_s\mathbf{W}^\perp + u_\parallel^s\epsilon_s\mathbf{W}^\parallel, \tag{6.16}$$

where

$$\mathbf{W}^\parallel = (\mathbf{W}\cdot\mathbf{m})\mathbf{m}, \qquad \mathbf{W}^\perp = (\mathbf{I} - \mathbf{mm})\cdot\mathbf{W}, \tag{6.17}$$

and $\Phi^0 = \Phi(\beta_{\text{D}}^0)$ is the hindered settling function for sedimentation evaluated at the unperturbed volume fraction β_{D}^0. In Paper I, the numerical results for this function were fitted by

$$\Phi(\beta_{\text{D}}) = (1-\beta_{\text{D}})^{c_1 - c_2\beta_{\text{D}}}, \tag{6.18}$$

with $c_1 = 6.50$, $c_2 = 3.18$. As before, the coefficients appearing in Eqs. (6.15) and (6.16) have a finite limit as $k\to 0$. From these expressions, we can calculate the tensors that arise in the right-hand side of Eq. (6.1) to find

$$\mathsf{S} = k\left[\mu_{\text{eff}}\frac{U^s}{a^2k^2} + \mu_\Delta u_\perp^s + \mu_\nabla \Phi^0 \beta_{\text{D}}^s - \mu_0 U^s\right]\epsilon_c \mathbf{G}_S^W + 2\left[\mu_\Delta u_\parallel^s + \mu_\nabla \Phi^0 \beta_{\text{D}}^s\right] k\epsilon_c \mathbf{G}_M^W, \tag{6.19}$$

where $\mathbf{G}_{S,\,M}^W$ are given by

$$\mathbf{G}_S^W = \mathbf{W}^\perp\mathbf{m} + \mathbf{m}\mathbf{W}^\perp, \qquad \mathbf{G}_M^W = (\mathbf{W}\cdot\mathbf{m})\left(\mathbf{m}\mathbf{m} - \frac{1}{3}\mathbf{I}\right). \tag{6.20}$$

The next step is to calculate S from its definition and to parameterize the results in the same form as in Eq. (6.19):

$$\frac{1}{\mu_{\text{C}}}\mathsf{S} = k\left(\frac{s_S^c}{a^2k^2}\mathbf{G}_S^W + s_M^c \mathbf{G}_M^W\right)\epsilon_c. \tag{6.21}$$

If, by analogy with Eq. (6.10), in this parameterization one were to introduce a term like $s_S^s\epsilon_s\mathbf{G}_S$, one finds numerically that $s_S^c = O(1)$, while $s_S^s = O(10^{-3})$. Hence, we feel justified in dropping such terms in Eq. (6.21).

Upon comparing with Eq. (6.19), we are led to

$$\frac{\mu_{\text{eff}}}{\mu_{\text{C}}}U^s + a^2k^2\left(\frac{\mu_\Delta}{\mu_{\text{C}}}u_\perp^s + \frac{\mu_\nabla}{\mu_{\text{C}}}\Phi^0\beta_{\text{D}}^s - \frac{\mu_0}{\mu_{\text{C}}}U^s\right) = s_S^c, \tag{6.22}$$

$$\frac{\mu_\Delta}{\mu_{\text{C}}}u_\parallel^s + \Phi^0\beta_{\text{D}}^s\frac{\mu_\nabla}{\mu_{\text{C}}} = \frac{1}{2}s_M^c. \tag{6.23}$$

These are the only two equations involving μ_∇. It is convenient for the following developments to use the second one to eliminate this quantity from the first one with the result

$$\frac{\mu_{\text{eff}}}{\mu_{\text{C}}}U^s + a^2k^2\left[\left(u_\perp^s - u_\parallel^s\right)\frac{\mu_\Delta}{\mu_{\text{C}}} - \frac{\mu_0}{\mu_{\text{C}}}U^s\right] = s_S^c - \frac{1}{2}a^2k^2s_M^c. \tag{6.24}$$

6.3. Couple

For the case in which a couple $\mathbf{T}$ acts on each particle, we have from Section 10 of Paper I:

$$\mathbf{u}_{\text{m}} - \mathbf{U}_\infty = \frac{U}{k}\epsilon_c\mathbf{m}\times\boldsymbol{\omega}, \tag{6.25}$$

$$\mathbf{u}_\Delta = a^2ku\epsilon_c\mathbf{m}\times\boldsymbol{\omega}. \tag{6.26}$$

Upon substitution into the closure relation (6.1) for S we find $\mathbf{E}_\nabla = O(\epsilon^2)$ and, therefore,

$$\mathsf{S} = -\left[\mu_{\text{eff}}U + a^2k^2(\mu_\Delta u - \mu_0 U)\right]\epsilon_s\mathbf{G}_S^\omega, \tag{6.27}$$

with $\mathbf{G}_S^\omega = (\mathbf{m}\times\boldsymbol{\omega})\mathbf{m} + \mathbf{m}(\mathbf{m}\times\boldsymbol{\omega})$. From the direct numerical calculation, on the other hand,

$$\mathsf{S} = s_S\epsilon_s\mu_{\text{C}}\mathbf{G}_S^\omega, \tag{6.28}$$

Table 1
Numerical values of the dimensionless effective viscosity $\mu_{\text{eff}}/\mu_{\text{C}}$ as determined from the three flow situations considered in this paper. Note the substantial consistency among the various results indicating the independence of this quantity from the particular flow considered

β_{D}^0 (%)	Eq. (6.11)	Eq. (6.33)	Eq. (6.34)	Eq. (6.35)
15	1.52	1.52	1.49	1.50
25	2.10	2.09	2.01	2.07
35	3.02	3.02	2.90	3.00

from which, upon comparing,

$$\frac{\mu_{\text{eff}}}{\mu_{\text{C}}}U + a^2k^2\left(\frac{\mu_\Delta}{\mu_{\text{C}}}u - \frac{\mu_0}{\mu_{\text{C}}}U\right) = -s_S. \tag{6.29}$$

6.4. The effective viscosities

Before drawing the consequences of the previous relations, it is important to remind the reader of the sense in which they must be understood. The closure relation (6.1) is proposed as a relation of general validity, independent of the particular flow considered (for a given particle probability distribution). Hence, the effective viscosities appearing in it will depend in general on the volume fraction[2] but not on the parameter k which, together with ϵ, $\mathbf{g}$, etc., characterizes the particular flow considered. For example, the dependence of S on k as expressed by Eq. (6.8) must arise from the k-dependence of the average fields (6.2) and (6.3) rather than directly from a k-dependence of the effective viscosities. This is another reason why we have inserted high-order terms such as $\nabla^2\mathbf{E}_{\text{m}}$ in Eq. (6.1). One could avoid this term by simply writing $\tilde{\mu}_{\text{eff}}\mathbf{E}_{\text{m}}$ in the closure relation, but this procedure would then lead to the k-dependent relation

$$\tilde{\mu}_{\text{eff}} = \mu_{\text{eff}} - (ak)^2\mu_0. \tag{6.30}$$

Retaining all the terms appearing in Eq. (6.1) has the effect of enabling us to treat the effective viscosities as constants, at least up to $O(ak)^2$ included.

The first relation (6.11) was examined in Paper I, where it was found that the expression in the right-hand side is independent of k and coincides with the effective viscosity of a uniform suspension as calculated by several authors (see e.g. Ladd, 1990; Mo and Sangani, 1994). Fig. 3 shows calculated values of $\mu_{\text{eff}}/\mu_{\text{C}}$ for several values of β_{D}^0 (circles; the segments will be explained later). Some numerical values are given in Table 1. The line is the fit

$$\frac{\mu_{\text{eff}}\left(\beta_{\text{D}}^0\right)}{\mu_{\text{C}}} = \left(1 - \frac{\beta_{\text{D}}^0}{\beta_{\max}}\right)^{-\theta}, \tag{6.31}$$

with $\beta_{\max} = 0.79$, $\theta = 1.94$ given in Paper I.

[2] In principle, of course, they will also depend on the particle probability distribution (see e.g. Zuzovsky et al., 1983) for which, however, a definite choice — randomly placed hard spheres — has been made in this study.

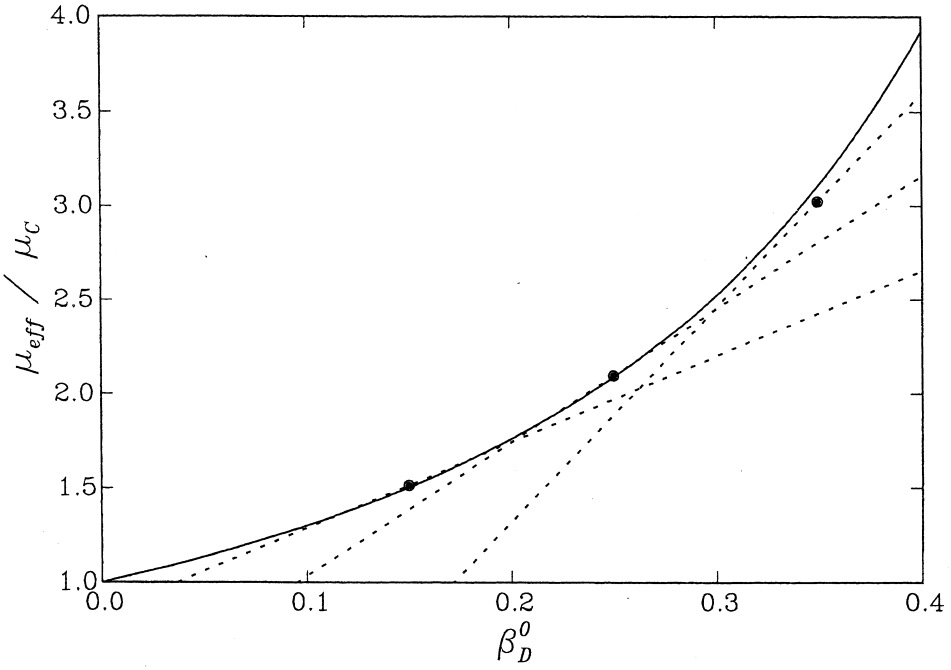

Fig. 3. The normalized effective viscosity $\mu_{\text{eff}}/\mu_{\text{C}}$ as a function of the disperse-phase volume fraction β_{D}^0.

Let us now consider the second relation (6.12). Since μ_{eff} is independent of k, so is its derivative. The left-hand side of the equation then suggests a quadratic interpolation $A + B(ak)^2$ for the right-hand side, which is compatible with the numerical results. In the limit $ak \to 0$, the term $a^2k^2(\mu_1/\mu_{\text{C}})$ in the left-hand side vanishes and what is left is the consistency condition

$$\frac{\mathrm{d}}{\mathrm{d}\beta_{\text{D}}}\left(\frac{\mu_{\text{eff}}}{\mu_{\text{C}}}\right) = \frac{1}{2}\lim_{k\to 0}\frac{s^s}{\beta_{\text{D}}^s}. \tag{6.32}$$

The values in the left-hand side can be found by differentiating (6.31) and, for $\beta_{\text{D}} = 15$, 25, and 35%, are 4.56, 7.52, and 13.7, respectively. The corresponding values of the right-hand side obtained from the least squares fit are instead 4.56, 7.11, and 11.3; the straight dashed lines in Fig. 3 have been drawn with these slopes. The agreement is excellent at the smaller volume fractions. The discrepancy for $\beta_{\text{D}}^0 = 35\%$ is somewhat larger but, as explained before, these results may not be as accurate due to the use of an insufficient number of singularities to represent the particles.

According to Eq. (6.12), the coefficient of the term $(ak)^2$, in the least-squares fit of the right-hand side should be identified with μ_1; some numerical values for this quantity are shown in Table 2. The dilute-limit result is $\mu_1/\mu_{\text{C}} = \frac{1}{4}\beta_{\text{D}}$.

By a similar argument, from Eq. (6.13) we deduce that, in the limit $ak \to 0$,

$$\frac{\mu_{\text{eff}}}{\mu_{\text{C}}} = -\frac{s_{S0}^s}{U_0^c}; \tag{6.33}$$

from Eq. (6.24)

$$\frac{\mu_{\mathrm{eff}}}{\mu_{\mathrm{C}}} = \frac{s^c_{S0}}{U^s_0}; \tag{6.34}$$

and, from Eq. (6.29),

$$\frac{\mu_{\mathrm{eff}}}{\mu_{\mathrm{C}}} = \frac{s_{S0}}{U_0}, \tag{6.35}$$

where, for brevity, we write

$$s^s_{S0} = \lim_{ak\to 0} s^s_S, \tag{6.36}$$

etc. These relations must be satisfied for the consistency of the present approach. The numerical values shown in Table 1 indicate that this is indeed so to a good accuracy. This remark is important as, on the one hand, it substantiates the correctness of the approach and, on the other, shows the independence of the effective viscosity from the particular flow considered (for a given particle probability distribution); this, of course, is an essential feature of an effective physical property appearing in a closure relation.

Eqs. (6.33)–(6.35) can be used to remove the k-independent terms from the corresponding Eqs. (6.13), (6.24), and (6.29) to find, after division by $(ak)^2$,

$$u^c_{\perp 0}\frac{\mu_\Delta}{\mu_{\mathrm{C}}} - U^c_0\frac{\mu_0}{\mu_{\mathrm{C}}} = -s^s_{S2} - \frac{\mu_{\mathrm{eff}}}{\mu_{\mathrm{C}}}U^c_2, \tag{6.37}$$

$$\left(u^s_{\perp 0} - u^s_{\parallel 0}\right)\frac{\mu_\Delta}{\mu_{\mathrm{C}}} - U^s_0\frac{\mu_0}{\mu_{\mathrm{C}}} = s^c_{S2} - \frac{1}{2}s^c_{M0} - \frac{\mu_{\mathrm{eff}}}{\mu_{\mathrm{C}}}U^s_2, \tag{6.38}$$

$$u_0\frac{\mu_\Delta}{\mu_{\mathrm{C}}} - U_0\frac{\mu_0}{\mu_{\mathrm{C}}} = -s_{S2} - \frac{\mu_{\mathrm{eff}}}{\mu_{\mathrm{C}}}U_2, \tag{6.39}$$

where

$$s^s_{S2} = \lim_{ak\to 0}\frac{s^s_S - s^s_{S0}}{(ak)^2}, \tag{6.40}$$

Table 2
Computed values of the effective viscosities μ_∇ and μ_1

β^0_{D} (%)	$\mu_\nabla/\mu_{\mathrm{C}}$	μ_1/μ_{C}
$O(\beta_{\mathrm{D}})$	0	$\frac{1}{4}\beta_{\mathrm{D}}$
15	1.17	0.228
25	2.65	0.495
35	7.39	1.05

Table 3
Calculated values of μ_Δ/μ_C for the three cases

β_D^0 (%)	Sedimentation	Couple	Shear
$O(\beta_D)$	–	–	$\frac{3}{5}\beta_D$
15	0.408	0.408	0.650
25	0.947	0.937	0.951
35	2.17	2.10	2.07

etc. Together with the $k = 0$ limit of Eq. (6.14), namely

$$\frac{\mu_\Delta}{\mu_C} = -\frac{s^s_{M0}}{2u^c_{\|0}}, \tag{6.41}$$

these are four equations in the two unknowns μ_Δ and μ_0. With a sufficient number of high-accuracy numerical simulations one should be able to solve any pair and find that the solution satisfies to a good accuracy the remaining two equations. Unfortunately, this straightforward approach is not available here because of the scatter of the numerical results that prevents a reliable determination of the fitting parameters. Hence, we take a less direct route as follows.

We first solve Eqs. (6.37) and (6.38) for μ_Δ, μ_0, and then Eqs. (6.38) and (6.39) for the same quantities. The two sets of values are similar, but not as close as it would be desirable. To improve this preliminary estimate we form a combination, f say, of the sums of the squares of the three Eqs. (6.37)–(6.39), and determine the fitting parameters on which f depends most strongly. This study reveals that these are $u^s_{\perp 0}$ and s^c_{M0}, and we therefore consider $f = f(u^s_{\perp 0}, s^c_{M0})$. We then increment these parameters by a small amount determined in such a way that the new value of f, approximated by the lowest-order Taylor series, vanishes. This procedure leads to new values for μ_Δ, μ_0 as computed from Eqs. (6.37), (6.38) and (6.38), (6.39) that are now very close to each other as shown in Tables 3 and 4. Finally, we verify whether the value of μ_Δ thus obtained is consistent with Eq. (6.41). Although, apparently, this is the simplest relation, it is unfortunately the one affected most strongly by the imprecision with which the fitting parameters can be determined.

This procedure could be improved in several ways, but at the cost of a significantly greater amount of work. Rather than proceeding in this direction, at this stage it appears more appropriate to wait for better numerical results obtained with a significantly larger number of particles and configurations. Such computations are currently under way. In any event, the results shown in Tables 3 and 4 already show a satisfactory degree of consistency. The numerical results can be fitted by[3]

[3] The exponents in these fits are close to 2 and one would be tempted to try a fit $\propto \beta_D^2$. The result is $\mu_\Delta/\mu_C = 16.80\beta_D^2$, $\mu_\nabla/\mu_C = 51.05\beta_D^2$, but the fit is not as good as that provided by Eq. (6.42).

Table 4
Calculated values of μ_0/μ_C for the three cases

β_D^0 (%)	Sedimentation	Couple	Shear
$O(\beta_D)$	–	–	$\frac{7}{80}\beta_D$
15	0.0218	0.0217	0.0410
25	0.0293	0.0301	0.0387
35	0.104	0.106	0.109

$$\frac{\mu_\Delta}{\mu_C} = 14.5\beta_D^{1.920}, \qquad \frac{\mu_\nabla}{\mu_C} = 61.5\beta_D^{2.128}; \tag{6.42}$$

These lines and the computed points are shown in Fig. 4.

In developing the previous considerations concerning terms of order $(ak)^2$ we have ignored the difficulty mentioned earlier of a possible contamination of the k-dependence by the underlying periodic structure. The degree of consistency among the numerical values calculated supports this procedure although, strictly speaking, the quantitative conclusions drawn in this section should be considered as tentative.

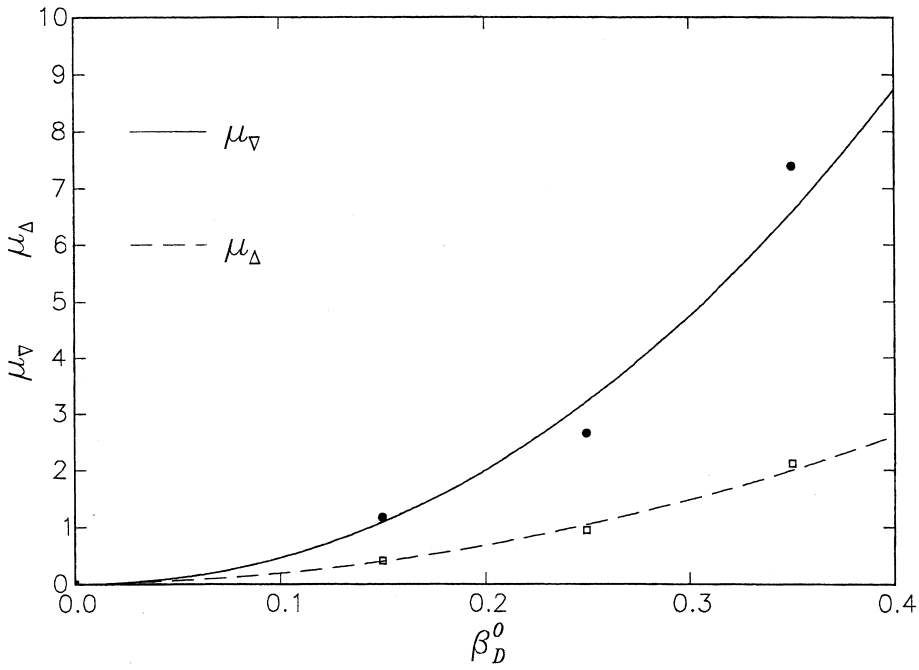

Fig. 4. The computed values of μ_Δ/μ_C (open circles) and μ_∇/μ_C (solid circles) as functions of β_D^0; the lines are the fits (6.42).

Table 5
Calculated values of Q_1, Q_2, V_1, R_1 for three volume fractions

β_D^0 (%)	Q_1	Q_2	V_1	R_1
15	0.260	1.150	0.00474	0.569
25	0.432	2.39	0.134	1.12
35	0.855	5.55	0.315	1.89

7. The isotropic part of the viscous stress

The isotropic part of the viscous stress must be closed in terms of the scalars (5.11), and we therefore write

$$\frac{1}{\mu_C} q_m = Q_1 \nabla \cdot \mathbf{u}_\Delta + Q_2 \mathbf{u}_\Delta \cdot \nabla \beta_D. \tag{7.1}$$

By using the expressions for $\mathbf{u}_\Delta$ given in the previous section, we find

$$\frac{1}{\mu_C} q_m = a^2 k^2 Q_1 u_\parallel^c (\mathbf{m} \cdot \boldsymbol{\gamma} \cdot \mathbf{m}) \epsilon_s + k \left(Q_1 u_\parallel^s + Q_2 \Phi^0 \beta_D \right) \epsilon_c \mathbf{W} \cdot \mathbf{m}, \tag{7.2}$$

where we have combined the two cases of shear and sedimentation for brevity; q_m vanishes to the present order in ϵ for the applied couple case.

An explicit expression for q_m in terms of averages of the local fields is given in Eq. (B.11) of Appendix B. As before, these averages are obtained from the numerical simulations and we parameterize them as

$$\frac{1}{\mu_C} q_m = a^2 k^2 q^\gamma \epsilon_s (\mathbf{m} \cdot \boldsymbol{\gamma} \cdot \mathbf{m}) + k q^W \epsilon_c \mathbf{W} \cdot \mathbf{m}. \tag{7.3}$$

Upon comparing with Eq. (7.2) we thus have

$$Q_1 = \lim_{k \to 0} \frac{q^\gamma}{u_\parallel^c}, \qquad Q_2 = \lim_{k \to 0} \frac{1}{\Phi^0 \beta_D^s} \left(q^W - \frac{u_\parallel^s}{u_\parallel^c} q^\gamma \right). \tag{7.4}$$

It is found numerically that, as a function of k, $u_\parallel^c$ goes through 0. To avoid a singularity it is therefore preferable to effect the extrapolation to $k = 0$ on β_D^0/Q_1, $1/Q_2$; the results of this operation are shown in Figs. 5 and 6, and numerical values are given in Table 5. As shown in Figs. 7 and 8 the numerical results can be fitted as[4]

$$Q_1 = 3.32 \beta_D^{1.371}, \qquad Q_2 = 34.5 \beta_D^{1.823} \tag{7.5}$$

It is clear that, if higher-order derivatives such as, for example, $\nabla^2(\nabla \cdot \mathbf{u}_\Delta)$, were retained in the

[4] An alternative, less good fit is provided by $Q_1 = 4.00 \beta_D^{3/2}$, $Q_2 = 44.6 \beta_D^2$.

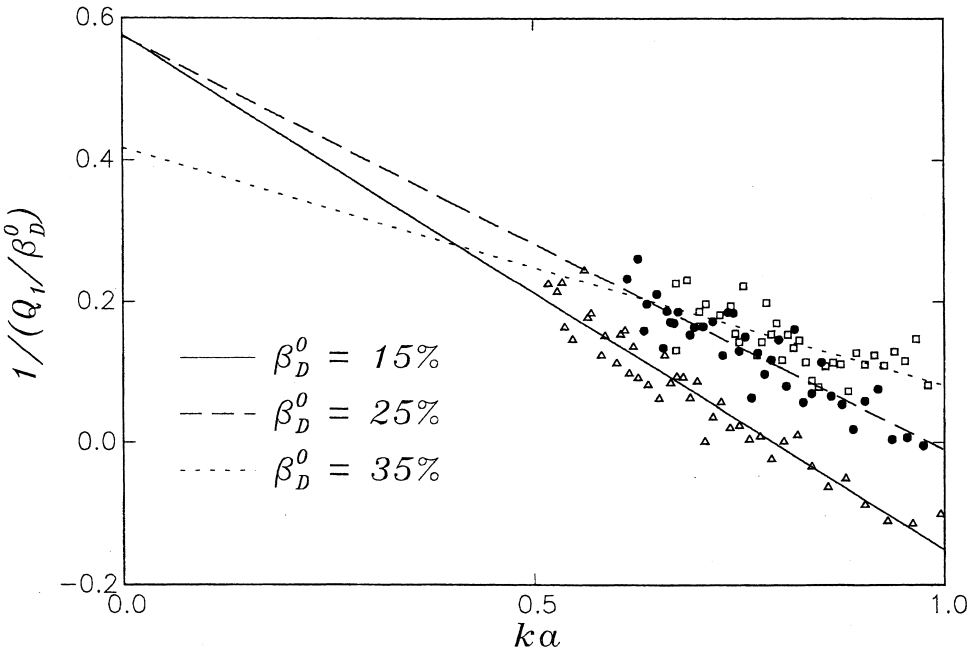

Fig. 5. The quantity β_{D}^0/Q_1 defined in Eq. (7.4) as a function of ka for $\beta_{\mathrm{D}}^0 = 15\%$ (triangles), 25% (black circles), and 35% (squares); the lines are least-squares linear fits.

closure (7.1), the corresponding contributions would have a higher order in k than those retained, and would therefore be unimportant in the limit $k \to 0$. The situation is thus different from that encountered in the previous section in which some terms with low-order derivatives gave a contribution of the same order in k as terms with higher-order derivatives. It is thus justified to retain only the low-order terms in the closure (7.1).

8. The antisymmetric part of the viscous stress

According to Eq. (2.8), the antisymmetric part of the stress can be expressed in terms of the polar vector V and of the axial vector R. The procedure is the same as that explained in detail in the previous sections and therefore an abbreviated description will be sufficient.

8.1. Closure of V

The vector V is polar and therefore, a priori, it can be expressed as a linear combination of the polar vectors listed in Section 5. Since it is the double curl of V that enters the final momentum equation, in order to avoid spatial velocity derivatives of order higher than the second, it would be sufficient to set V simply proportional to $\mathbf{u}_\Delta$. Nevertheless, we shall also include higher-order polar vectors much for the same reason as in the symmetric part of the viscous stress in Section 6, namely because some terms that would give a negligible

contribution to the averaged equations appear to have the same order in k as $\mathbf{u}_\Delta$ for some of the flows that we simulate. Furthermore, by so doing, we shall derive consistency relations useful as a check of the results. Thus, we postulate the following closure relation:

$$\frac{1}{\mu_C}\mathsf{V} = V_1\mathbf{u}_\Delta + V_2a^2\mathbf{E}_m\cdot\nabla\beta_D + V_3a^2\nabla^2\mathbf{u}_m + V_4a^2\nabla\times\boldsymbol{\Omega}_\Delta + V_5a^2\nabla\beta_D\times\boldsymbol{\Omega}_\Delta$$
$$+ a^2V_6\nabla(\nabla\cdot\mathbf{u}_\Delta) + a^2V_7(\mathbf{u}_\Delta\cdot\nabla)\nabla\beta_D + a^2V_8\mathbf{u}_\Delta\nabla^2\beta_D + a^2V_9\nabla^2\mathbf{u}_\Delta. \tag{8.1}$$

Expressions for $\mathbf{u}_\Delta$ and $\mathbf{u}_m$ for the three cases were given in the previous section. In order to proceed, we need to give corresponding expressions for $\boldsymbol{\Omega}_\Delta$ which are the following:

$$\boldsymbol{\Omega}_\Delta = k\Omega^c\mathbf{m}\times\mathbf{W}\epsilon_c \quad \text{sedimentation,} \tag{8.2}$$

$$\boldsymbol{\Omega}_\Delta = a^2k^2\Omega^s\epsilon_s\mathbf{m}\times\boldsymbol{\gamma}^\perp, \quad \text{shear,} \tag{8.3}$$

$$\boldsymbol{\Omega}_\Delta = \Psi\boldsymbol{\omega} + \left(\Omega_\parallel\boldsymbol{\omega}^\parallel + \Omega_\perp\boldsymbol{\omega}^\perp\right)\epsilon_s \quad \text{couple,} \tag{8.4}$$

where

$$\boldsymbol{\omega}^\perp = \boldsymbol{\omega} - (\mathbf{m}\cdot\boldsymbol{\omega})\mathbf{m}, \qquad \boldsymbol{\omega}^\parallel = (\mathbf{m}\cdot\boldsymbol{\omega})\mathbf{m}. \tag{8.5}$$

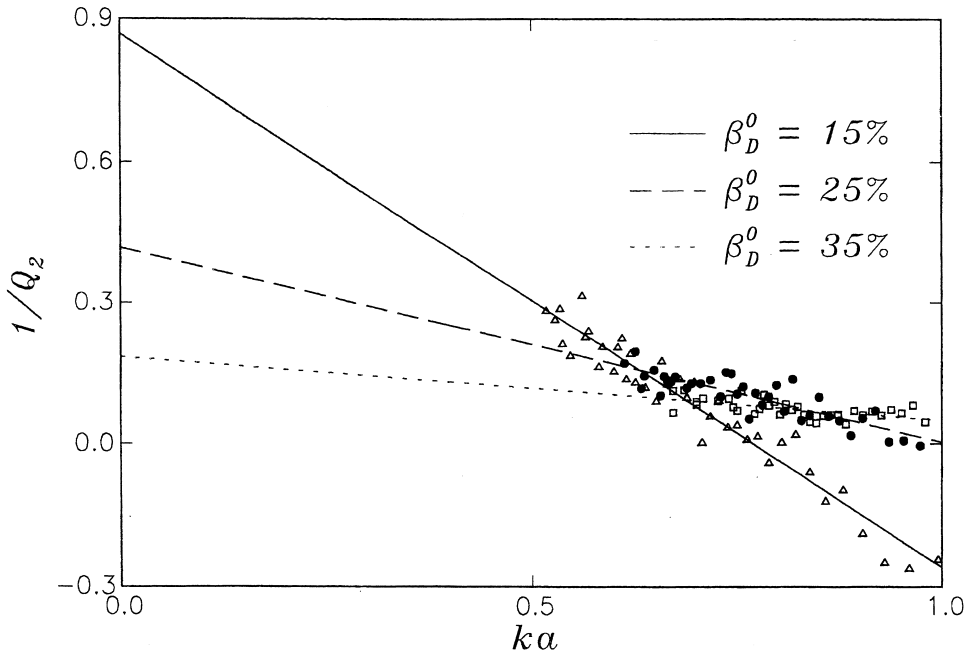

Fig. 6. The quantity $1/Q_2$ defined in Eq. (7.4) as a function of ka for $\beta_D^0 = 15\%$ (triangles), 25% (black circles), and 35% (squares); the lines are least-squares linear fits.

In Eq. (8.4), $\Psi(\beta_D)$ is the hindrance function for rotation introduced in Paper I (see also Brenner, 1970; Brenner, 1984), where it was fitted as

$$\Psi = \left(1 - \beta_D\right)^{c_3 - c_4\beta_D}, \tag{8.6}$$

with $c_3 = 1.50$, $c_4 = 0.41$.

From a parameterization of the direct numerical results for V calculated from the expression (B.16) we find, in the three cases,

$$\frac{1}{\mu_C}\mathsf{V} = v^0\mathbf{W} + \left(v_\parallel^s\mathbf{W}^\parallel + v_\perp^s\mathbf{W}^\perp\right)\epsilon_s, \tag{8.7}$$

$$\frac{1}{\mu_C}\mathsf{V} = a^2k\left(v_\parallel^c\boldsymbol{\gamma}^\parallel + v_\perp^c\boldsymbol{\gamma}^\perp\right)\epsilon_c, \tag{8.8}$$

$$\frac{1}{\mu_C}\mathsf{V} = a^2kv^c\mathbf{m}\times\boldsymbol{\omega}\epsilon_c. \tag{8.9}$$

With these expressions and the earlier ones for $\mathbf{u}_\Delta$ and $\mathbf{u}_m$ we have, for sedimentation,

$$\Phi^0 V_1 = v^0, \tag{8.10}$$

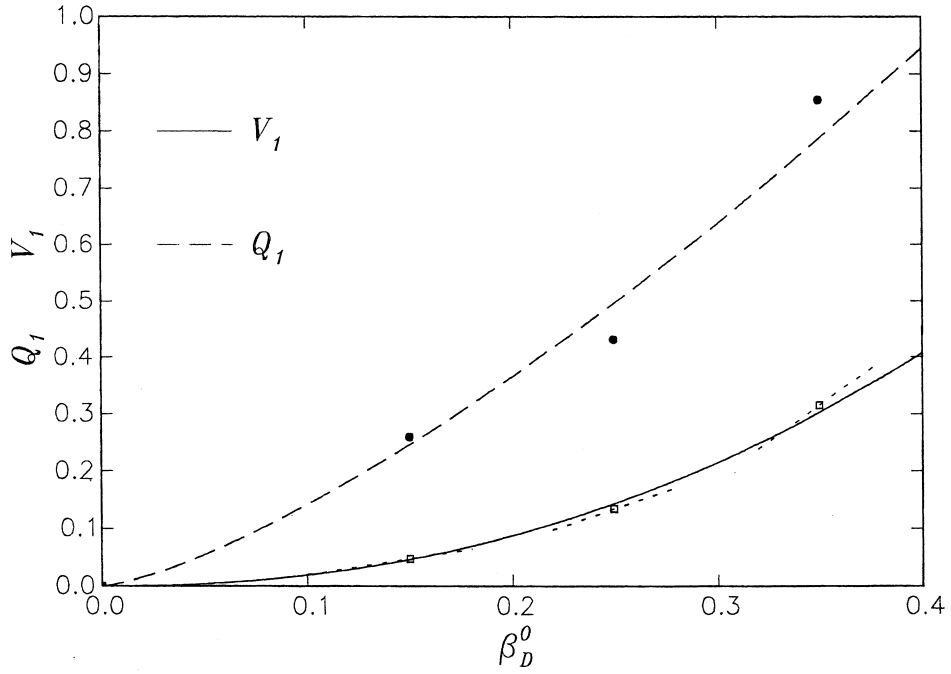

Fig. 7. The computed values of Q_1 (solid circles) and V_1 (open circles) as functions of β_D^0; the lines are the fits (7.5) and (8.16).

$$\Phi^0\frac{\mathrm{d}V_1}{\mathrm{d}\beta_\mathrm{D}}+\frac{u^s_\parallel}{\beta^s_\mathrm{D}}V_1=-\frac{v^s_\parallel}{\beta^s_\mathrm{D}}+\frac{a^2k^2}{\beta^s_\mathrm{D}}\Big[u^s_\parallel(V_6+V_9)+\Phi^0\beta^s_\mathrm{D}(V_7+V_8)\Big], \tag{8.11}$$

$$-\Phi^0\frac{\mathrm{d}V_1}{\mathrm{d}\beta_\mathrm{D}}-\frac{u^s_\perp}{\beta^s_\mathrm{D}}V_1+\frac{U^s}{\beta^s_\mathrm{D}}V_3=\frac{v^s_\perp}{\beta^s_\mathrm{D}}+\frac{a^2k^2}{\beta^s_\mathrm{D}}\big(\Omega^cV_4-\Phi^0\beta^s_\mathrm{D}V_8-u^s_\perp V_9\big), \tag{8.12}$$

for the shear case

$$\frac{u^c_\parallel}{\beta^s_\mathrm{D}}V_1+V_2=-\frac{v^c_\parallel}{\beta^s_\mathrm{D}}+a^2k^2\frac{u^c_\parallel}{\beta^s_\mathrm{D}}(V_6+V_9), \tag{8.13}$$

$$\frac{u^c_\perp}{\beta^s_\mathrm{D}}V_1+V_2-\frac{U^c}{\beta^s_\mathrm{D}}V_3=-\frac{v^c_\perp}{\beta^s_\mathrm{D}}+\frac{a^2k^2}{\beta^s_\mathrm{D}}\big(\Omega^sV_4+u^s_\perp V_9\big), \tag{8.14}$$

and for the applied couple

$$\frac{1}{\beta^s_\mathrm{D}}(uV_1-UV_3)+\frac{\Omega_\perp}{\beta^s_\mathrm{D}}V_4+\Psi^0V_5=-\frac{v^c}{\beta^s_\mathrm{D}}+\frac{a^2k^2}{\beta^s_\mathrm{D}}uV_9. \tag{8.15}$$

As before, we write $\Phi^0=\Phi(\beta^0_\mathrm{D})$ and $\Psi^0=\Psi(\beta^0_\mathrm{D})$.

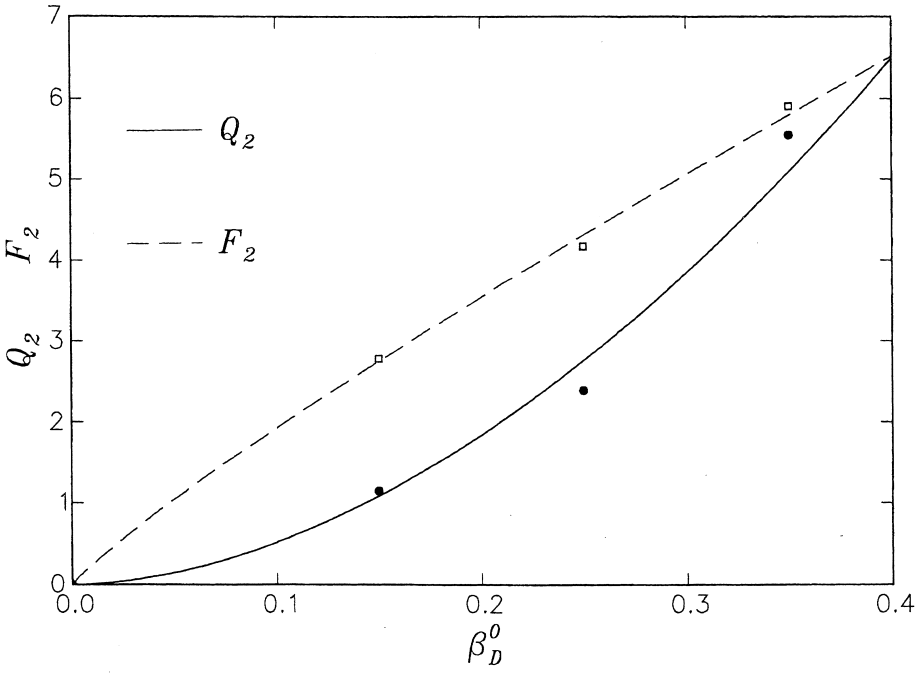

Fig. 8. The computed values of Q_2 (solid circles) and F_2 (open circles) as functions of β^0_D; the lines are the fits (7.5) and (9.16).

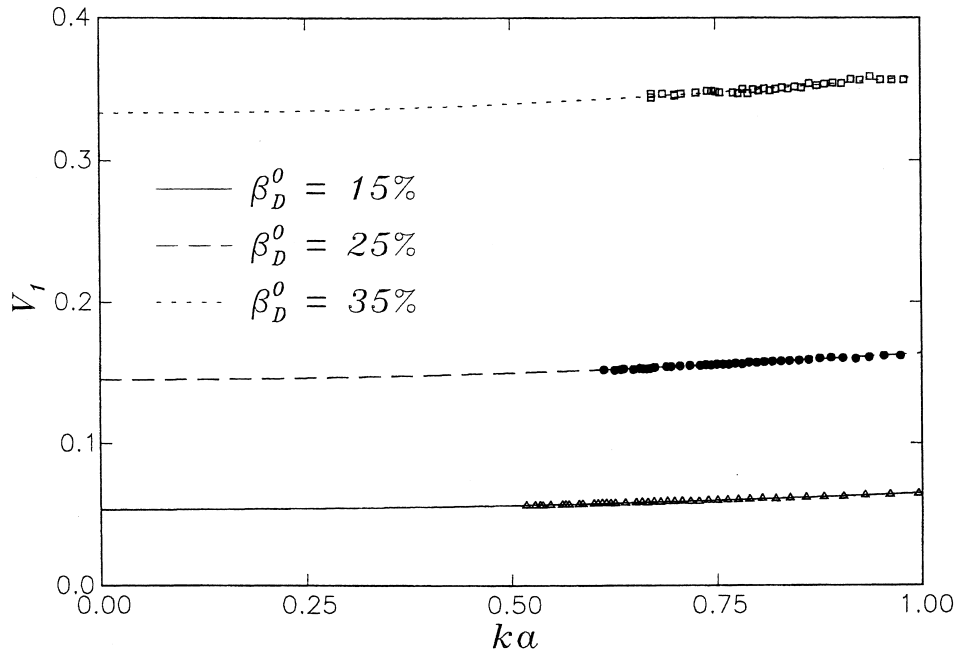

Fig. 9. The quantity V_1 given by Eq. (8.10) as a function of ka for $\beta_D^0 = 15\%$ (triangles), 25% (black circles), and 35% (squares); the lines are least-squares linear fits.

The first relation (8.10) only involves homogeneous averages and it is found numerically that v^0 is independent of k. Upon using the value of Φ^0 extrapolated to $k = 0$, we thus evaluate V_1 in the same limit. The dependence of V_1 upon ak is shown in Fig. 9 and the values extrapolated to $ak = 0$ are plotted as a function of β_D in Fig. 7. The dashed line is a fit of the form[5]

$$V_1 = 3.11\beta_D^{2.219}. \tag{8.16}$$

By evaluating the second relation (8.11) in the limit $ak \to 0$ we find

$$\Phi^0 \frac{dV_1}{d\beta_D} + \frac{u_\parallel^s}{\beta_D^s} V_1 = -\frac{v_\parallel^s}{\beta_D^s}, \tag{8.17}$$

which is a consistency condition similar to Eq. (6.32) encountered earlier. As in that case, we fit the k-dependent numerical results by the quadratic $A + B(ak)^2$ and extrapolate to $ak = 0$. It is found that the scatter is very small with B of the order of a few percent of A so that, the extrapolation can be carried out with confidence. Segments with a slope given by this extrapolation are attached to the calculated values of $V_1(\beta_D)$ in Fig. 7. It appears that these slopes are consistent with the trend of the results. Numerically, for $\beta_D = 15\%$, the two sides of Eq. (8.17) equal 0.0937 and 0.0985, respectively; for $\beta_D = 25\%$ 0.0571 and 0.0624; for $\beta_D = 35\%$ 0.0400 and 0.0391.

[5] Another, not as good, possibility with a simpler exponent is $V_1 = 3.25\beta_D^{9/4}$.

Eq. (8.13) evaluated for $k = 0$ can be used to find V_2; with V_1 and V_2 known, one can find expressions for V_3 from both, Eqs. (8.12) and (8.15). We will not show these results as the corresponding terms, when inserted in the momentum equation, would contain spatial derivatives of order beyond the second.

8.2. Closure of R

It is the curl of R that enters the momentum equation and, in order to have second-order velocity derivatives at the most, first-order derivatives in R would be sufficient. Nevertheless, as before, we include second-order terms as well. On the basis of the analysis of Section 5, we set

$$\frac{1}{\mu_C}\mathsf{R} = R_1\boldsymbol{\Omega}_\Delta + R_2 a^2 \nabla \times \left(\mathbf{E}_m \cdot \nabla\beta_D\right) + R_3 a^2 \nabla^2(\nabla \times \mathbf{u}_m) + R_4 \nabla \times \mathbf{u}_\Delta + R_5 \nabla\beta_D \times \mathbf{u}_\Delta$$
$$+ R_6 a^2 \nabla(\nabla \cdot \boldsymbol{\Omega}_\Delta) + R_7 a^2 (\boldsymbol{\Omega}_\Delta \cdot \nabla)\nabla\beta_D + a^2 R_8 \boldsymbol{\Omega}_\Delta \nabla^2 \beta_D + a^2 R_9 \nabla^2 \boldsymbol{\Omega}_\Delta. \tag{8.18}$$

By calculating R according to its expression (B.15) and suitably parameterizing the results, we find, for the case of sedimentation,

$$\frac{1}{\mu_C}\mathsf{R} = k r^c \mathbf{m} \times \mathbf{W}\epsilon_c, \tag{8.19}$$

for the case of shear

$$\frac{1}{\mu_C}\mathsf{R} = a^2 k^2 r^s \mathbf{m} \times \boldsymbol{\gamma}^\perp \epsilon_s, \tag{8.20}$$

and, for the applied couple,

$$\frac{1}{\mu_C}\mathsf{R} = r^0 \boldsymbol{\omega} + \left(r^s_\parallel \boldsymbol{\omega}^\parallel + r^s_\perp \boldsymbol{\omega}^\perp\right)\epsilon_s. \tag{8.21}$$

By comparing with Eq. (8.18), in which suitable substitutions are made for the primary variables $\mathbf{u}_m$, $\mathbf{u}_\Delta$, etc., we have

$$\Omega^c R_1 - R_3 U^s + R_4 u^s_\perp + \Phi^0 \beta^s_D R_5 = r^c + a^2 k^2 \Omega^c R_9, \tag{8.22}$$

for sedimentation,

$$\Omega^s R_1 - \beta^s_D R_2 + U^c R_3 - u^c_\perp R_4 = r^s + a^2 k^2 \Omega^s R_9, \tag{8.23}$$

for shear, and

$$\Psi^0 R_1 = r^0, \tag{8.24}$$

$$\Omega_\parallel R_1 + \Psi^0 \beta^s_D \frac{dR_1}{d\beta_D} = r^s_\parallel + a^2 k^2 \left[\Omega_\parallel (R_6 + R_9) + \Psi^0 \beta^s_D (R_7 + R_8)\right], \tag{8.25}$$

$$\Omega_\perp R_1 + \Psi^0 \beta_D^s \frac{dR_1}{d\beta_D} - a^2 k^2 (UR_3 - uR_4) = r_\perp^s + a^2 k^2 \left(\Psi^0 \beta_D^s R_8 + \Omega_\perp R_9\right), \tag{8.26}$$

for the applied couple.

It will be shown below in Eq. (9.24) that $\Omega_\parallel = \Omega_\perp$ so that, for consistency of Eqs. (8.25) and (8.26) in the limit $k \to 0$, one must have $r_\parallel^s = r_\perp^s$, which is indeed numerically verified. From the first term in the expression (B.15) for R, from the expression (B.18) for the hydrodynamic couple, and from the definition (4.8) of $\boldsymbol{\omega}$, it can be shown that r^0 in the right-hand side of Eq. (8.24) equals $3\beta_D^0$ so that the first equation (8.24) simply shows that

$$R_1(\beta_D) = 3\frac{\beta_D}{\Psi(\beta_D)}, \tag{8.27}$$

where, as mentioned before, Ψ is the rotational hindrance function for a uniform suspension. By using this relation in Eq. (8.25) or (8.26), again in the limit $k \to 0$, we find

$$3\frac{\beta_D^0}{\Psi^0}\left(\Omega_\parallel - \beta_D^s \frac{d\Psi}{d\beta_D}\right) = r_\parallel^s - 3\beta_D^s. \tag{8.28}$$

From Eq. (9.24) derived later, the left-hand side vanishes. The numerical evidence for the right-hand side is consistent with this conclusion.

Unfortunately, the remaining equations are insufficient to calculate the other closure constants, and in particular R_4 and R_5, that multiply terms that would make a contribution in the momentum equation. In order to determine these coefficients it appears necessary to simulate other flow situations.

9. The inter-phase interaction force and couple

In view of the vectorial nature of the interphase interaction force $\mathbf{f}$, on the basis of the considerations of Section 5, we may represent it as

$$v\mathbf{f} = 6\pi\mu_C a^3 \beta_C \big[a^{-2} F_1 \mathbf{u}_\Delta + F_2 \mathbf{E}_m \cdot \nabla\beta_D + F_3 \nabla^2 \mathbf{u}_m + F_4 \nabla \times \boldsymbol{\Omega}_\Delta + F_5 \nabla\beta_D \times \boldsymbol{\Omega}_\Delta$$
$$+ F_6 \nabla(\nabla \cdot \mathbf{u}_\Delta) + F_7 (\mathbf{u}_\Delta \cdot \nabla)\nabla\beta_D + F_8 \mathbf{u}_\Delta \nabla^2 \beta_D + F_9 \nabla^2 \mathbf{u}_\Delta\big]. \tag{9.1}$$

Contrary to the previous cases in which the quantity to be closed had to be suitably parameterized on the basis of numerical results, here we readily find an exact analytical expression. For this purpose, we eliminate $\mathbf{f}$ between the momentum equations (2.5) and (2.6) to find

$$\nabla(-p_m + \boldsymbol{\Sigma}_C) = -\left(\beta_C \rho_C + \beta_D \rho_D\right)\mathbf{g}. \tag{9.2}$$

Upon substitution into the disperse-phase momentum equation (2.5) we then find (with $\mathbf{U}_\infty = 0$)

$$v\mathbf{f} = 6\pi a \mu_C \beta_C \mathbf{W}. \tag{9.3}$$

In the couple and shear cases **g** vanishes and, from Eq. (4.6), so does **W**. In these cases, therefore, **f** = 0. We also recall from Paper I, Eq. 8.1, the definition of the hindered settling function Φ,

$$\mathbf{u}_\Delta = \Phi(\beta_D)\mathbf{W}, \tag{9.4}$$

and note that, as in Eq. (6.7),

$$F_1(\beta_D)\mathbf{u}_\Delta = \left[F_1\left(\beta_D^0\right) + \frac{dF_1}{d\beta_D}\beta_D^s\epsilon_s\right]\mathbf{u}_\Delta + O(\epsilon^2). \tag{9.5}$$

With these results and the earlier expressions for $\mathbf{u}_\Delta$, $\mathbf{u}_m$, and $\boldsymbol{\omega}_\Delta$ we find, for sedimentation,

$$\Phi^0 F_1 = 1, \tag{9.6}$$

$$u_\parallel^s F_1 + \Phi^0\frac{dF_1}{d\beta_D}\beta_D^s = -a^2k^2\left[u_\parallel^s(F_6+F_9) + \Phi^0\beta_D^s(F_7+F_8)\right], \tag{9.7}$$

$$u_\perp^s F_1 + \Phi^0\frac{dF_1}{d\beta_D}\beta_D^s + U^s F_3 = a^2k^2\left(\Omega^c F_4 - \Phi^0\beta_D^s F_8 - u_\perp^s F_9\right), \tag{9.8}$$

for shear

$$u_\parallel^c F_1 - \beta_D^s F_2 = -a^2k^2 u_\parallel^c(F_6+F_9), \tag{9.9}$$

$$u_\perp^c F_1 - \beta_D^s F_2 + U^c F_3 = -a^2k^2\left(\Omega^s F_4 + u_\perp^c F_9\right), \tag{9.10}$$

and for the applied couple

$$uF_1 + UF_3 - \Omega_\perp F_4 - \Psi^0\beta_D^s F_5 = -a^2k^2 uF_9. \tag{9.11}$$

The number of equations is smaller than the number of unknowns which therefore cannot all be determined. We limit ourselves to the terms of order 0 in ak and drop all terms of order a^2k^2.

Eq. (9.6) shows that F_1 is the inverse of the hindered settling function Φ, which simply follows from the definition of this quantity; a fit to the numerical results was given earlier in Eq. (6.18). When Eq. (9.6) is used to eliminate F_1 in Eq. (9.7), neglecting the terms of order $(ak)^2$, one has

$$u_\parallel^s = \frac{d\Phi}{d\beta_D}\beta_D^s. \tag{9.12}$$

Similarly, from Eqs. (9.8) and (9.10),

$$F_3 = \frac{u_\parallel^s - u_\perp^s}{U^s\Phi^0}, \qquad F_3 = \frac{u_\parallel^c - u_\perp^c}{U^c\Phi^0}, \tag{9.13}$$

Table 6
Computed values for some of the closure terms for the force and the hydrodynamic couple

β_D^0 (%)	F_2	F_3	L_1
15	2.78	0.380	1.14
25	4.17	0.666	2.24
35	5.91	1.26	3.77

while, from Eq. (9.9),

$$F_2 = \frac{u_\parallel^c}{\beta_D^s \Phi^0}. \tag{9.14}$$

It is understood that all the coefficients in these relations are evaluated in the limit $k \to 0$.

The relation (9.12) can be checked since $u_\parallel^s$ is found from a fit to the numerical results while the right-hand side is calculated from Eq. (6.18). For $\beta_D^0 = 15$, 25, and 35%, one finds $u_\parallel^s = -0.345$, -0.313, and -0.238, while $(d\Phi/d\beta_D)\beta_D^s = -0.370$, -0.324, and -0.238. The agreement is quite satisfactory. For $\beta_D = 15\%$, the right-hand sides of the two expression for F_3 (9.13) are found to converge to the values 0.370 and 0.389 as $ak \to 0$. These numbers are sufficiently close to be considered equal within the accuracy that can be expected in the present calculations. The situation is similar for 25 and 35%, where one finds $F_3 = 0.668$, 0.664 and 1.38, 1.13, respectively. In the dilute limit, F_3 is the coefficient of the Faxén term in the force and therefore equals 1/6. The three computed values plus $F_3 = 1/6$ for $\beta_D^0 = 0$ are shown in Table 6 and Fig. 10, where the line is a fit of the form

$$F_3 = \frac{1}{6} + 6.777\beta_D^{1.767}. \tag{9.15}$$

It can be seen that the computed values are consistent with the analytical result at $\beta_D^0 = 0$. Finally, from Eq. (9.14), one can evaluate F_2 with the results given in Table 6 and shown in Fig. 8; the line is the fit[6]

$$F_2 = 14.6\beta_D^{0.8822}. \tag{9.16}$$

As in the previous cases, it is impossible to determine the remaining coefficients using only the results of the three flows simulated in this study.

If the k-independent terms are subtracted from the two sides of Eq. (9.12) and the result divided by ak, one has a relation that is not verified numerically. We believe that this circumstance is due to the fact that the k dependence of Φ is contaminated by the periodic cell structure of the suspension, as indicated by the fact (already mentioned in Section 4) that Φ is found to depend on k even in the uniform case. Short of an analytical proof, a fully satisfactory resolution of this matter requires the use of different spatial periods for the spatial

[6] Alternatively, F_2 and F_3 can be fitted as $F_2 = 17.35\beta_D$, $F_3 = \frac{1}{6} + 9.49\beta_D^2$. The quality of these fits is however somewhat inferior.

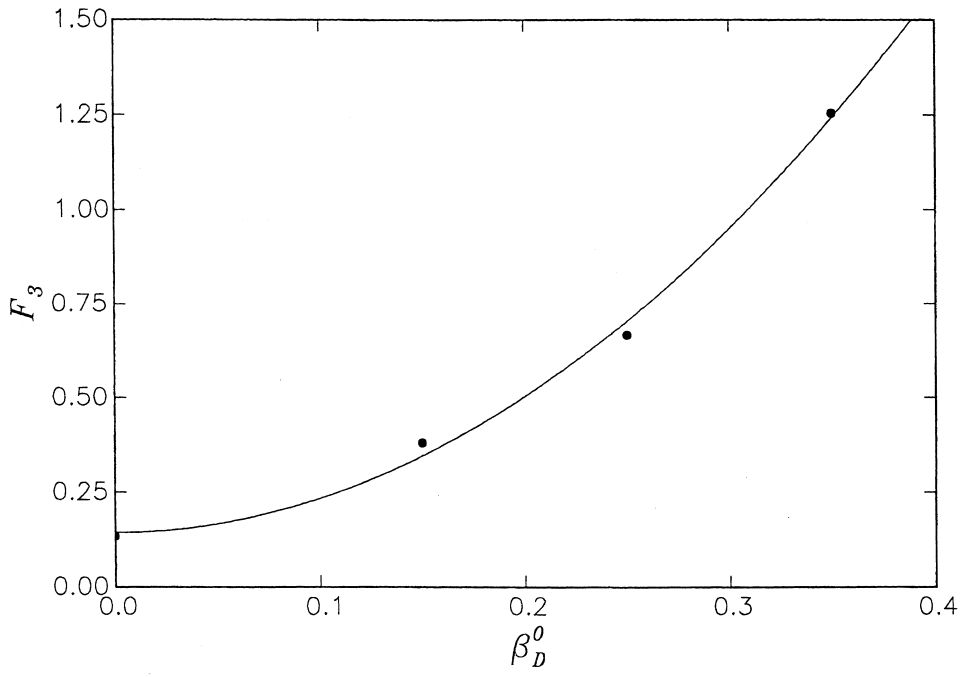

Fig. 10. The parameter F_3 given by Eq. (9.13) as a function of β_{D}^0; the line is the fit (9.15).

non-uniformity and the fundamental cell structure of the suspension, as discussed in Section 4. Unfortunately, the conspicuous computational resources necessary for this task are beyond those presently available to us.

The last quantity that needs to be closed is the hydrodynamic couple acting on the particles. This is an axial vector and can therefore be closed similarly to Eq. (8.18):

$$\frac{n}{\mu_{\mathrm{C}}}\overline{\int_{|\mathbf{r}|=a} \mathrm{d}S\mathbf{r}\times(\boldsymbol{\sigma}_{\mathrm{C}}\cdot\mathbf{n})}$$
$$= -L_1\boldsymbol{\Omega}_\Delta + L_2a^2\nabla\times\left(\mathbf{E}_m\cdot\nabla\beta_{\mathrm{D}}\right) + L_3a^2\nabla^2(\nabla\times\mathbf{u}_{\mathrm{m}}) + L_4\nabla\times\mathbf{u}_\Delta + L_5\nabla\beta_{\mathrm{D}}\times\mathbf{u}_\Delta$$
$$+ L_6a^2\nabla(\nabla\cdot\boldsymbol{\Omega}_\Delta) + L_7a^2(\boldsymbol{\Omega}_\Delta\cdot\nabla)\nabla\beta_{\mathrm{D}} + a^2L_8\boldsymbol{\Omega}_\Delta\nabla^2\beta_{\mathrm{D}} + a^2L_9\nabla^2\boldsymbol{\Omega}_\Delta. \tag{9.17}$$

The angular momentum balance equation shows that the integral in the left-hand side equals minus the applied couple and therefore vanishes for sedimentation and shear. Proceeding as before, we therefore find

$$-\Omega^cL_1 - U^sL_3 + u_\perp^sL_4 + \Phi^0\beta_{\mathrm{D}}^sL_5 = a^2k^2\Omega^cL_9, \tag{9.18}$$

for the case of sedimentation

$$-\Omega^sL_1 - \beta_{\mathrm{D}}^sL_2 + U^cL_3 - u_\perp^cL_4 = a^2k^2\Omega^sL_9, \tag{9.19}$$

for shear, and

$$\Psi^0 L_1 = 6\beta_{\mathrm{D}}^0, \tag{9.20}$$

$$-\Omega_{\parallel} L_1 - \Psi^0 \beta_{\mathrm{D}}^s \frac{\mathrm{d}L_1}{\mathrm{d}\beta_{\mathrm{D}}} = -6vn^s + a^2k^2\left[\Omega_{\parallel}(L_6 + L_9) + \Psi^0 \beta_{\mathrm{D}}^s (L_7 + L_8)\right], \tag{9.21}$$

$$-\Omega_{\perp} L_1 - \Psi^0 \beta_{\mathrm{D}}^s \frac{\mathrm{d}L_1}{\mathrm{d}\beta_{\mathrm{D}}} = -6vn^s + a^2k^2\left(UL_3 - uL_4 + \Psi^0 \beta_{\mathrm{D}}^s L_8 + \Omega_{\perp} L_9\right), \tag{9.22}$$

for the applied couple. Eq. (9.20), which follows from the definition of the hindrance function for rotation (see e.g. Eq. 10.1 in Paper I) shows that $L_1(\beta_{\mathrm{D}}^0) = 6\beta_{\mathrm{D}}^0/\Psi^0 = 2R_1$. Upon eliminating L_1 between Eqs. (9.21) and (9.22), in the limit $k \to 0$, one finds

$$\Omega_{\parallel} = \Omega_{\perp} = \beta_{\mathrm{D}}^s \frac{\mathrm{d}\Psi}{\mathrm{d}\beta_{\mathrm{D}}}. \tag{9.23}$$

The three quantities appearing here are shown in Table 7 where a good consistency is observed. Again, it is not possible to determine the other coefficients.

10. Discussion and conclusions

In this paper, we have developed a method to deduce closure relations for the averaged equations describing a spatially non-uniform disperse two-phase flow of equal spheres in a viscous fluid. The method is systematic and relies on an averaging procedure to reduce the closure quantities to numerical coefficients multiplying the primary average fields and their derivatives. The coefficients have been calculated on the basis of extensive numerical simulations.

The constitutive relations determined have been presented in Sections 6–9. Due to the manner of their derivation, some of these relations would give rise to spatial derivatives of velocities of order higher than 2 when substituted into the momentum equations. Such terms represent effects of higher order in the ratio of the particle radius to the macroscopic length scale, and can be expected to be small. Furthermore, their presence would render necessary the formulation of new boundary conditions to be used for the solution of the equations. For these reasons it seems reasonable to drop them, at least for the time being. With this simplification,

Table 7
Numerical values of the quantities appearing in the consistency relation (9.22)

β_{D}^0 (%)	$-\Omega_{\parallel}$	$-\Omega_{\perp}$	$-\beta_{\mathrm{D}}^s(\mathrm{d}\Psi/\mathrm{d}\beta_{\mathrm{D}})$
15	0.218	0.211	0.193
25	0.340	0.332	0.292
35	0.429	0.416	0.373

collecting the previous results, the final expression for the viscous stress becomes

$$\boldsymbol{\Sigma}_{\mathrm{C}} = -\big(Q_1\nabla\cdot\mathbf{u}_\Delta + Q_2\mathbf{u}_\Delta\cdot\nabla\beta_{\mathrm{D}}\big)\mathbf{I} + 2\mu_{\mathrm{eff}}\mathbf{E}_{\mathrm{m}} + 2\mu_\Delta\mathbf{E}_\Delta + 2\mu_\Delta\mathbf{E}_\nabla + \mu_{\mathrm{C}}\boldsymbol{\epsilon}\cdot\big[R_1\boldsymbol{\Omega}_\Delta + R_4\nabla \times \mathbf{u}_\Delta + R_5\nabla\beta_{\mathrm{D}}\times\mathbf{u}_\Delta - \nabla(V_1\mathbf{u}_\Delta)\big], \tag{10.1}$$

where $\boldsymbol{\epsilon}$ is the completely antisymmetric three-tensor. Here, $\mathbf{u}_\Delta = \bar{\mathbf{w}} - \mathbf{u}_{\mathrm{m}}$ is the particle "slip" velocity and $\boldsymbol{\Omega}_\Delta = \bar{\boldsymbol{\Omega}} - \frac{1}{2}\nabla\times\mathbf{u}_{\mathrm{m}}$ the slip rotational velocity; $\mathbf{E}_\Delta$ is the rate of strain of the field $\mathbf{u}_\Delta$ and $\mathbf{E}_{\mathrm{m}}$ the analogous tensor related to the mixture volumetric flux $\mathbf{u}_{\mathrm{m}}$ defined in Eq. (A.1); $\mathbf{E}_\nabla$ is defined in Eq. (5.9). The effective viscosity μ_{eff} is the same as that found by earlier investigators; μ_Δ and μ_∇ are other viscosities the values of which are given in Tables 2 and 3 for particle volume fractions $\beta_{\mathrm{D}} = 15$, 25, and 35%. Section 9 describes closures for the hydrodynamic force and couple acting on the particles.

In addition to the viscosities, the constitutive relation (10.1) contains several other volume-fraction-dependent coefficients such as, R_1, R_4, etc. for the determination of which a sufficient number of relations is required. By considering three different flow situations — sedimentation, shear, and applied couple — we were able to generate some of the required relations. The missing ones will require the simulation of other flows.

Even though the closure method that we have developed is systematic, it is not exact. We quantify the non-homogeneity of the particle distribution in terms of a small parameter and use a perturbation expansion in terms of this parameter truncated to first order. In principle, one could carry other orders (and in practice at least one more) to gain further information. This approach might be useful also to attack flows with small, but non-zero, particle Reynolds number.

A significant practical difficulty that we have encountered is that our method requires a consideration of the limit of large cell sizes L (or, more precisely, of $ka\to 0$, where a is the particle radius and $k = 2\pi/L$). Approaching this limit requires in turn a relatively large number of particles in the fundamental cell, while we were limited to a maximum of about 60 by the computational resources at our disposal. Secondly, convergence of the ensemble averaging is very slow and, even with 1000 or more configurations for each computed point, some of our results were plagued by a significant statistical noise. We expect that faster computers and better algorithms (e.g., that of Sangani and Mo, 1996 or another one under development in our group) would make a significant difference. We hope to be able to refine the present calculations in the near future.

A fundamental limitation of the method as presented in this paper lies in the use of an assumed probability distribution — randomly arranged hard-spheres — that is not correct for a flowing suspension (Batchelor and Green, 1972; Brady and Morris, 1997). Whether the present approach can be extended to deal with a more realistic particle probability distribution is, at present, an open question. However, on the basis of a similar experience with homogeneous suspensions where the particle probability distribution affects the numerical value of the effective viscosity but not the Newtonian nature of the rheological constitutive relation, it might be expected that at least the functional form of the equations that we have found would remain valid.

In spite of these limitations, an interesting conclusion of the present study — that can be

expected to be independent of the probability distribution — is the qualitative difference between uniform and non-uniform suspensions. A spatial non-homogeneity confers to the suspension rheological properties that cannot be inferred on the basis of those of a homogeneous one.

An important task still ahead is of course the numerical solution of the averaged equations. It is only in this way that one can judge the effect and importance of the various terms and, most importantly, compare with experiment. It might also be possible to determine some of the closure parameters by comparing the results of such simulations with experimental data or direct numerical simulations.

It was shown in both this paper and in Paper I that, in a non-uniform suspension, an interphase slip velocity develops even in situations (e.g., uniform shear) for which no such slip would exist in the uniform case. This result hints at the possibility that the closure relations derived here might contain the phenomenon of shear-induced particle migration. Since we have an explicit momentum equation for the particle phase, this effect would appear here not as diffusion, but as the response of the particles to deterministic (average) forces[7]. A similar conclusion has been reached by other means by Nott and Brady (1994). In order to verify this conjecture, it will be necessary to wait until solutions of the averaged equations become available.

Acknowledgements

This study has been supported by NSF under grant CTS-9521373 and by the Engineering Research Program of the Office of Basic Energy Sciences at the Department of Energy under grant Nos. DE-FG02-89ER14043 and DE-FG02-99ER14966.

Appendix A. Definitions

We collect here several definitions relating to the quantities introduced in Section 2.

The mean volumetric flow rate $\mathbf{u}_m$ may be written as

$$\mathbf{u}_m = \beta_C \langle \mathbf{u}_C \rangle + \beta_D \langle \mathbf{u}_D \rangle, \tag{A.1}$$

where $\mathbf{u}_{C,D}$ are the velocities of the phases and the ensemble averages, indicated by angle brackets, and are defined by

$$\beta_{C,D} \langle \mathbf{u}_{C,D} \rangle (\mathbf{x}, t) = \frac{1}{N!} \int \mathrm{d}\mathscr{C}^N \chi_C(\mathbf{x}; N) \mathbf{u}_{C,D}(\mathbf{x}, t; N) P(N, t). \tag{A.2}$$

Here the notation $\mathbf{u}_{C,D}(\mathbf{x}, t; N)$ stresses the fact that the instantaneous velocities at point $\mathbf{x}$ and time t are evaluated when the N particles are in the configuration $\mathscr{C}^N$. It should be noted

[7] One would expect that a description in terms of diffusion would be recovered by deriving an approximate relation for $\mathbf{u}_\Delta$ from the particle momentum equation and substituting it into the particle number equation (2.2).

that the disperse-phase average velocity $\langle \mathbf{u}_D \rangle$ is different from the particle average velocity $\mathbf{w}$ that is defined by

$$n(\mathbf{x}, t)\bar{\mathbf{w}}(\mathbf{x}, t) = \frac{1}{N!}\int \mathrm{d}C^N P(N)\left[\sum_{\alpha=1}^{N}\delta(\mathbf{x}-\mathbf{y}^\alpha)\mathbf{w}^\alpha(N)\right]$$

$$= \frac{1}{(N-1)!}\int \mathrm{d}\mathscr{C}^{N-1} P(\mathbf{x}, \mathbf{w}, N-1)\mathbf{w}^1(\mathbf{x}, \mathbf{w}, N-1) \tag{A.3}$$

in which $\mathbf{w}^\alpha$ is the velocity of the αth particle. The difference consists in the fact that $\langle \mathbf{u}_D \rangle$ is the mean velocity of all the particle material contained in the unit volume, while $\bar{\mathbf{w}}$ is the mean velocity of the particle centers of mass contained in the unit volume. The two quantities are of course equal in a spatially uniform suspension. In general, however, they are related by

$$\beta_D\langle \mathbf{u}_D \rangle = \left(1 + \frac{\alpha^2}{10}\nabla^2 + \frac{a^4}{280}\nabla^4 + \cdots\right)(nv\bar{\mathbf{w}}) + \frac{a^2}{5}\left(1 + \frac{a^2}{14}\nabla^2 + \cdots\right)\nabla \times (nv\bar{\boldsymbol{\Omega}}), \tag{A.4}$$

where $\bar{\boldsymbol{\Omega}}$ is the particle-average angular velocity. In a similar way, β_D is not exactly equal to nv:

$$\beta_D = \left(1 + \frac{a^2}{10}\nabla^2 + \frac{a^4}{280}\nabla^4 + \cdots\right)(nv). \tag{A.5}$$

According to the results of Paper II, the mixture pressure p_m is given by

$$p_m = \beta_C\langle p_C \rangle + \left(1 + \frac{a^2}{10}\nabla^2\right)\left[nv\overline{p^e}\right] + \frac{1}{5}a^2\nabla\cdot\left[n\overline{\int_{|\mathbf{r}|=a}\mathrm{d}S(-\mathbf{n})p_C}\right]$$

$$+ \frac{1}{14}a^2\nabla\nabla:\left[n\overline{\int_{|\mathbf{r}|=a}\left(\mathbf{nn} - \frac{1}{3}\mathbf{I}\right)p_C}\right] + \cdots. \tag{A.6}$$

Here p_C is the continuous-phase pressure, $\langle p_C \rangle$ is defined as in Eq. (A.2), the integrals are over the surface of the particles, and the quantity $\overline{p^e}$ is the average of the mean pressure over the particle surface defined by

$$p^e(\mathbf{x}, t; N) = \frac{1}{4\pi a^2}\int_{|\mathbf{r}|=a}\mathrm{d}S_r p_C(\mathbf{x}+\mathbf{r}, t|N). \tag{A.7}$$

The various particle averages in Eq. (A.6) are defined as in Eq. (A.3).

When adapted to the present case of constant hydrodynamic force, the expression given in Eq. (5.33) of Paper II for the symmetric part of the stress S is

$$S = \beta_C(\langle \boldsymbol{\sigma}_C \rangle + \langle p_C \rangle \mathbf{I}) + \left(1 + \frac{a^2}{14}\nabla^2\right)(n\mathbf{t}^s) + \nabla(n\mathbf{s}^s) + \nabla\nabla:(n\mathbf{r}^s), \tag{A.8}$$

where $\mathbf{t}^s$, $\mathbf{s}^s$, and $\mathbf{r}^s$ are tensors related to moments of the traction at the particle surface and expressible in terms of averages of Lamb coefficients as shown in Appendix B. Specifically, $\mathbf{t}^s$ is

the stresslet given by

$$t^{\mathrm{s}}_{ij} = \frac{1}{2}\left(\mathscr{T}^0_{ij} + \mathscr{T}^0_{ji}\right), \tag{A.9}$$

with

$$\mathscr{T}^0_{ji} = a\overline{\int_{|\mathbf{r}|=a} \mathrm{d}S_r \left[n_j(\boldsymbol{\sigma}_{\mathrm{C}} \cdot \mathbf{n})_i - \frac{1}{3}\delta_{ij}(\mathbf{n} \cdot \boldsymbol{\sigma}_{\mathrm{C}} \cdot \mathbf{n}) \right]}. \tag{A.10}$$

Similarly,

$$s^s_{kji} = \frac{1}{2}\left(\mathscr{S}^0_{kji} + S^0_{kij}\right) - \frac{1}{3}\delta_{ij}\mathscr{S}^0_{kmm}, \tag{A.11}$$

$$r^s_{lkji} = \frac{1}{2}\left(\mathscr{R}^0_{lkji} + \mathscr{R}^0_{lkij}\right) - \frac{1}{3}\delta_{ij}\mathscr{R}^0_{lkmm}. \tag{A.12}$$

with

$$\mathscr{S}^0_{kji} = \frac{1}{2}a^2\overline{\int_{|\mathbf{r}|=a} \mathrm{d}S_r \left[n_k n_j(\boldsymbol{\sigma}_{\mathrm{C}} \cdot \mathbf{n})_i - \frac{1}{5}\left(\delta_{ij}(\mathbf{n} \cdot \boldsymbol{\sigma}_{\mathrm{C}})_k + \delta_{kj}(\mathbf{n} \cdot \boldsymbol{\sigma}_{\mathrm{C}})_i + \delta_{ki}(\mathbf{n} \cdot \boldsymbol{\sigma}_{\mathrm{C}})_j\right) \right]}, \tag{A.13}$$

$$\mathscr{R}_{lkji} = \frac{1}{6}a^3\overline{\int_{|\mathbf{r}|=a} \mathrm{d}S_r n_l n_k n_j(\boldsymbol{\sigma}_{\mathrm{C}} \cdot \mathbf{n})_i}, \tag{A.14}$$

$$\mathscr{R}^0_{lkji} = \mathscr{R}_{lkji} - \frac{a^2}{84}\delta_{ijklpq}\mathscr{T}^0_{pq} + \frac{a^2}{30}v\delta_{ijkl}\overline{p^e} \tag{A.15}$$

In Zhang and Prosperetti (1997) it was also shown that, for rigid particles,

$$\beta_{\mathrm{C}}\langle\boldsymbol{\sigma}_{\mathrm{C}}\rangle = -\beta_{\mathrm{C}}\langle p_{\mathrm{C}}\rangle\mathbf{I} + 2\mu_{\mathrm{C}}\mathbf{E}_{\mathrm{m}}. \tag{A.16}$$

The average total hydrodynamic force on the particles is

$$\mathscr{A} = \overline{\int_{|\mathbf{r}|=a} \mathrm{d}S\boldsymbol{\sigma}_{\mathrm{C}} \cdot \mathbf{n}}. \tag{A.17}$$

The antisymmetric part of the stress is

$$\mathsf{A}_{ji} = \frac{1}{2}n\left(\mathscr{T}^0_{ji} - \mathscr{T}^0_{ij}\right) + \partial_k\left[\frac{1}{2}n\left(\mathscr{S}^0_{kji} - \mathscr{S}^0_{kij}\right)\right] + \partial_l\partial_k\left[\frac{1}{2}n\left(\mathscr{R}^0_{lkji} - \mathscr{R}^0_{lkij}\right)\right], \tag{A.18}$$

and the isotropic part

$$q_{\mathrm{m}} = \frac{a^2}{5}\nabla(n\mathscr{A}^*) - \frac{a^2}{14}\partial_k\partial_l\left(nt^s_{kl}\right)^* + \frac{1}{15}a^2 n\nabla\cdot\mathscr{A} - \partial_k\left(ns^i_{kmm}\right) - \partial_l\partial_k\left(nr^i_{lkmm}\right), \tag{A.19}$$

where $\mathscr{A}^*$, $(t^s)^*$ denote the part of $\mathscr{A}$, $\mathbf{t}^s$ arising from the viscous stresses, i.e.

$$\mathscr{A}^* = \overline{\int_{|\mathbf{r}|=a} \mathrm{d}S(\boldsymbol{\sigma}_C + p_C\mathbf{I}) \cdot \mathbf{n}}, \tag{A.20}$$

$$T_{ji}^{*0} = a\overline{\int_{|\mathbf{r}|=a} \mathrm{d}S_r \left\{ n_j\left[(\boldsymbol{\sigma}_C + p_C\mathbf{I}) \cdot \mathbf{n}\right]_i - \frac{1}{3}\delta_{ij}\left[\mathbf{n}(\boldsymbol{\sigma}_C + p_C\mathbf{I}) \cdot \mathbf{n}\right]\right\}}. \tag{A.21}$$

Appendix B. Explicit expressions

The relations of Appendix A are general and are valid whether or not the local particle Reynolds number is small. If the particles are immersed in a local Stokes flow, more specific expressions in terms of the local microscopic fields near the particles can be obtained. Here we present such explicit expressions which make it possible in practice to evaluate the averages numerically.

If the sphere α is immersed in Stokes flow, an exact solution for the flow fields is known in the form (Lamb, 1932; Kim and Karrila, 1991):

$$p_C^\alpha = \mu_C \sum_{-\infty}^{\infty} p_n^\alpha, \tag{B.1}$$

$$\mathbf{u}_C^\alpha = \sum_{-\infty}^{\infty}\left[\frac{1}{(n+1)(2n+3)}\left(\frac{1}{2}(n+3)r^2\nabla p_n^\alpha - np_n^\alpha\mathbf{r}\right) + \nabla\phi_n^\alpha + \nabla\left(\mathbf{r}\chi_n^\alpha\right)\right], \tag{B.2}$$

where each one of the p_n^α, ϕ_n^α, and χ_n^α is a spherical harmonic of order n, $\mathbf{r} = \mathbf{x} - \mathbf{y}^\alpha$ is the distance from the particle center and $r = |\mathbf{r}|$. Here and in the following we follow the notation of Mo and Sangani (1994) to whose paper the reader is referred for details.

With these expressions, the surface integrals appearing in the definition (A.6) of the mixture pressure given in the previous section can be calculated with the results

$$\overline{p^e} = \overline{p_0}, \tag{B.3}$$

$$\overline{\int_{|\mathbf{r}|=a} \mathrm{d}S\mathbf{n}p_C} = v\overline{\nabla r^3 p_{-2}} - \frac{30}{a^2}v\overline{\nabla r^3\phi_{-2}^*}, \tag{B.4}$$

$$\overline{\int_{|\mathbf{r}|=a} \mathrm{d}S\left(\mathbf{nn} - \frac{1}{3}\mathbf{I}\right)p_C} = \frac{a^2}{5}v\overline{\nabla\nabla r^5 p_{-3}} - \frac{21}{2}v\overline{\nabla\nabla r^5\phi_{-3}^*}. \tag{B.5}$$

Here and in the following the notation implies that all the r-dependent quantities are evaluated at the particle center $\mathbf{r} = 0$ after taking the derivatives with respect to $\mathbf{r}$. Inserting these expression into Eq. (A.6) we find

$$p_{\mathrm{m}} = \beta_{\mathrm{C}}\langle p_{\mathrm{C}}\rangle + \left(1 + \frac{a^2}{10}\nabla^2\right)(nv\overline{p_0}) - \frac{a^2}{5}\nabla\left[nv\overline{\nabla r^3 p_{-2}} - \frac{a^2}{14}\nabla\cdot\left(nv\overline{\nabla\nabla r^5 p_{-3}}\right)\right]$$
$$+ 6\nabla\left[nv\overline{\nabla r^3\phi^*_{-2}} - \frac{a^2}{8}\nabla\left(nv\overline{\nabla\nabla r^5\phi^*_{-3}}\right)\right]. \tag{B.6}$$

The other quantities introduced in the previous section can also be calculated explicitly. The results are

$$t^s_{ij} = -\frac{2}{3}\pi\overline{\partial_j\partial_i\left(r^5 p_{-3}\right)}, \tag{B.7}$$

$$s^s_{kji} = \frac{v}{2a}\overline{\left(\delta_{jk}\partial_i + \delta_{ik}\partial_j - \frac{2}{3}\delta_{ij}\partial_k\right)\left[\frac{3}{a^2}\left(r^3\phi^*_{-2}\right) + \frac{1}{5}\left(r^3 p_{-2}\right)\right]} + \frac{v}{30a^3}\overline{\partial_k\partial_j\partial_i\left(r^7 p_{-4}\right)}, \tag{B.8}$$

$$r^s_{lkji} = \frac{v}{24a^3}\overline{\left[3\left(\delta_{ik}\partial_j\partial_l + \delta_{jk}\partial_i\partial_l + \delta_{il}\partial_j\partial_k + \delta_{jl}\partial_i\partial_k\right) - 4\left(\delta_{ij}\partial_k\partial_l + \delta_{kl}\partial_i\partial_j\right)\right]\left(r^5\phi^*_{-3}\right)}$$
$$+ \frac{v}{28.35a}\overline{\left[\frac{8}{3}\delta_{ij}\partial_k\partial_l - 9\delta_{kl}\partial_i\partial_j - 2\left(\delta_{ik}\partial_j\partial_l + \delta_{jk}\partial_i\partial_l + \delta_{il}\partial_j\partial_k + \delta_{jl}\partial_i\partial_k\right)\right]\left(r^5 p_{-3}\right)}$$
$$- \frac{v}{840a^3}\overline{\partial_l\partial_k\partial_j\partial_i\left(r^9 p_{-5}\right)}, \tag{B.9}$$

where

$$\phi^*_{-n-1} = \phi_{-n-1} - \frac{a^2}{4n+2}p_{-n-1}. \tag{B.10}$$

The isotropic part q_{m} is found to be

$$q_{\mathrm{m}} = \frac{2}{15}a^2\nabla\left[nv\overline{\nabla\left(r^3 p_{-2}\right)}\right] - \frac{1}{5}a^2 nv\nabla\cdot\overline{\nabla\left(r^3 p_{-2}\right)} + 2\nabla\left[nv\overline{\nabla\left(r^3\phi^*_{-2}\right)}\right]$$
$$- \frac{1}{70}a^4\nabla\nabla{:}\left[nv\overline{\nabla\nabla\left(r^5 p_{-3}\right)}\right] - \frac{1}{2}a^2\nabla\nabla{:}\left[nv\overline{\nabla\nabla\left(r^5\phi^*_{-3}\right)}\right]. \tag{B.11}$$

The combinations arising in the antisymmetric part (A.18) are

$$\frac{1}{2}\left(\mathscr{T}^0_{ij} - \mathscr{T}^0_{ji}\right) = \frac{3v}{a^2}\epsilon_{ijm}\overline{\partial_m\left(r^3\chi_{-2}\right)}, \tag{B.12}$$

$$\frac{1}{2}\left(\mathscr{S}^0_{kji} - \mathscr{S}^0_{kij}\right) = \frac{v}{2a}\overline{\left(\delta_{jk}\partial_i - \delta_{ki}\partial_j\right)\left(\frac{1}{5}r^3 p_{-2} + \frac{3}{a^2}r^3\phi^*_{-2}\right)} - \frac{v}{a^3}\epsilon_{ijm}\overline{\partial_k\partial_m\left(r^5\chi_{-3}\right)}, \tag{B.13}$$

$$\frac{1}{2}\left(\mathscr{R}^0_{lkji} - \mathscr{R}^0_{lkij}\right) = \frac{3v}{10a}\delta_{lk}\epsilon_{ijm}\overline{\partial_m\left(r^3\chi_{-2}\right)} + \frac{v}{10a^3}\epsilon_{ijm}\overline{\partial_l\partial_k\partial_m\left(r^7\chi_{-4}\right)}. \tag{B.14}$$

Upon comparing with Eq. (2.8), $\mathsf{A}_{ij}=\varepsilon_{ijm}(\mathsf{R}_{\mathrm{m}}-\varepsilon_{mqr}\partial_q \mathsf{V}_r)$, one immediately finds

$$\mathsf{R}=\frac{3}{a^2}\left(1+\frac{a^2}{10}\nabla^2\right)\left(nv\overline{\nabla\left(r^3\chi_{-2}\right)}\right)-\nabla\left[\frac{nv}{a^3}\overline{\nabla\nabla\left(r^5\chi_{-3}\right)}\right]$$
$$+\nabla\nabla:\left[\frac{nv}{10a^3}\overline{\nabla\nabla\nabla\partial_{\mathrm{m}}\left(r^7\chi_{-4}\right)}\right], \tag{B.15}$$

$$\mathsf{V}=-\frac{nv}{2a}\left[\frac{1}{5}\overline{\nabla\left(r^3p_{-2}\right)}+\frac{3}{a^2}\overline{\nabla\left(r^3\phi^*_{-2}\right)}\right]. \tag{B.16}$$

Finally, we give the expression of the total mean hydrodynamic force on the particles:

$$\mathscr{A}[\boldsymbol{\sigma}_{\mathrm{C}}]=-4\pi a\mu_{\mathrm{C}}\overline{\nabla r^3p_{-2}}. \tag{B.17}$$

and for the total mean hydrodynamic couple:

$$\frac{1}{\mu_{\mathrm{C}}}\overline{\int_{|\mathbf{r}|=a}\mathrm{d}S\mathbf{r}\times(\boldsymbol{\sigma}_{\mathrm{C}}\cdot\mathbf{n})}=3v\overline{\nabla r^3\chi_{-2}}. \tag{B.18}$$

References

Ahmed, A.M. and Elghobashi, S.E., 1999. Direct numerical simulation of particle dispersion in homogeneous turbulent shear flows. Phys. Fluids, in press.

Batchelor, G.K., Green, J.T., 1972. The determination of the bulk stress in a suspension of spherical particles to order c^2. J. Fluid Mech. 56, 401–427.

Brady, J.F., Morris, J.F., 1997. Microstructure of strongly sheared suspensions and its impact on rheology and diffusion. J. Fluid Mech. 348, 103–139.

Brenner, H., 1970. Rheology of a dilute suspension of dipolar spherical particles in an external field. J. Colloid Interface Sci. 32, 141–158.

Brenner, H., 1984. Antisymmetric stress induced by the rigid-body rotation of dipolar suspensions. Int. J. Engng. Sci. 22, 645–682.

Glowinsky, R., Pan, T.W., Hesla, T.I., Joseph, D.D., 1999. A distributed Lagrange multiplier/fictitious domain method for particulate flows. Int. J. Multiphase Flow 25, 755–794.

Hu, H.H., 1996. Direct simulation of flows of solid-liquid mixtures. Int. J. Multiphase Flow 22, 335–352.

Johnson, A.A., Tezduyar, T., 1997. 3-D simulation of fluid-particle interactions with the number of particles reaching 100. Comp. Meth. Appl. Mech. Engng. 145, 301–321.

Kang, S.Y., Sangani, A.S., Tsao, H.K., Koch, D.L., 1997. Rheology of dense bubble suspensions. Phys. Fluids 9, 1540–1561.

Kim, S., Karrila, S.J., 1991. Microhydrodynamics. Butterworth-Heinemann, Boston.

Koch, D.L., Ladd, A.J.C., 1997. Moderate Reynolds number flow through periodic and random arrays of aligned cylinders. J. Fluid Mech. 349, 31–66.

Ladd, A.J.C., 1990. Hydrodynamic transport coefficients of random dispersions of hard spheres. J. Chem. Phys. 93, 3484–3494.

Ladd, A.J.C., 1997. Sedimentation of homogeneous suspensions of non-Brownian spheres. Phys. Fluids 9, 491–499.

Lamb, H., 1932. Hydrodynamics, 6th ed. Cambridge University Press, Cambridge.

Marchioro, M., Prosperetti, A., 1999. Conduction in non-uniform composites. Proc. R. Soc. London A455, 1483–1508.

Marchioro, M., Tanksley, M., and Prosperetti, A., 2000. Flow of spatially non-uniform suspensions. Part I: Phenomenology. Int. J. Multiphase Flow, 26, 783–831.

Marchioro, M., Tanksley, M., Prosperetti, A., 1999. Mixture pressure and stress in disperse two-phase flow. Int. J. Multiphase Flow 25, 1395–1430.

Mo, G., Sangani, A.S., 1994. A method for computing Stokes flow interactions among spherical objects and its application to suspensions of drops and porous particles. Phys. Fluids 6, 1637–1652.

Morris, J.F., Brady, J.F., 1998. Pressure-driven flow of a suspension: buoyancy effects. Int. J. Multiphase Flow 24, 105–130.

Nobari, M.R.H., Tryggvason, G., 1996. Numerical simulations of three-dimensional drop collisions. AIAA J. 34, 750–755.

Nott, P.R., Brady, J.F., 1994. Pressure-driven flow of suspensions: simulation and theory. J. Fluid Mech. 275, 157–199.

Pan, Y., Banerjee, S., 1997. Numerical investigation of the effect of large particles on wall turbulence. Phys. Fluids 9, 3786–3807.

Phung, T.N., Brady, J.F., Bossis, G., 1996. Stokesian dynamics simulation of Brownian suspensions. J. Fluid Mech. 313, 181–207.

Sangani, A.S., Mo, G.B., 1996. An $O(N)$ for Stokes and Laplace interactions of spheres. Phys. Fluids 8, 1990–2010.

Sangani, A.S., Mo, G.B., Tsao, H.K., Koch, D.L., 1996. Simple shear flow of dense gas-solid suspensions at finite Stokes numbers. J. Fluid Mech. 313, 309–341.

Sangani, A.S., Yao, C., 1988. Bulk conductivity of composites with spherical inclusions. J. Appl. Phys. 63, 1334–1341.

Stock, D.E., 1996. Particle dispersion in flowing gases. J. Fluids Engr. 118, 4–17.

Studart, N., da Silveira, H.V., de Freitas, U., 1996. Effective field theory for hard-sphere fluids. Phys. Rev. E53, 2350–2354.

Throop, G.J., Bearman, R.J., 1965. Numerical solution of the Percus–Yevick equation for the hard-sphere potential. J. Chem. Phys. 42, 2408–2411.

Torquato, S., Lee, S.B., 1990. Computer simulations of nearest-neighbor distribution function and related quantities for hard-sphere systems. Physica A 167, 361–383.

Zhang, D.Z., Prosperetti, A., 1994. Averaged equations for inviscid disperse two-phase flow. J. Fluid Mech. 267, 185–219.

Zhang, D.Z., Prosperetti, A., 1997. Momentum and energy equations for disperse two-phase flows and their closure for dilute suspensions. Int. J. Multiphase Flow 23, 425–453.

Zuzovsky, M., Adler, P.M., Brenner, H., 1983. Spatially periodic suspensions of convex particles in linear shear flows. Part III: Dilute arrays of spheres suspended in newtonian fluids. Phys. Fluids 26, 1714–1723.